The University of South Bohemia in České Budějovice

Faculty of Science

Water isotopes in dissolved organic matter: the interface of isotope hydrology and organic geochemistry

Bachelor thesis

Niclas Zehetner

Supervisor: Travis Blake Meador, Ph.D.

České Budějovice 2024

Zehetner, N., 2024: Water isotopes in dissolved organic matter: the interface of isotope hydrology and organic geochemistry. Bc. Thesis, in English. – 47 p., Faculty of Science, University of South Bohemia, České Budějovice, Czech Republic

Annotation

To investigate dissolved organic matter cycling in the pristine Lake Plešné in the Bohemian Forest, samples were collected from four locations over the course of approximately one hydrological year using different solid phase extraction techniques and analysed for recovery percentage, chromophoric properties, and stable carbon, hydrogen, and oxygen isotopic composition.

I declare that I am the author of this qualification thesis and that in writing it I have used the sources and literature displayed in the list of used sources only.

České Budějovice, …… ……
Niclas Zehetner

Acknowledgements

I would like to thank my supervisor, Travis Blake Meador, Ph. D., for guiding me in writing my bachelor thesis, for his invaluable insights, and for being patient with me. Additionally, I would like to thank Petr Porcal, Ph D. for conducting the DOC and EEM analysis. I am also grateful to Karelys Umbria Salinas for guiding me in the laboratory, and the SOWA IRMS team for their kind assistance in laboratory protocols and analyses. Finally, I would like to thank my family and friends for supporting me throughout my studies.

Abstract

Dissolved organic matter (DOM) is an important component of the global carbon cycle, constituting up to 55% of the total terrestrial carbon transported from the continents to the oceans. Despite extensive scientific effort, the cycling and fluxes of DOM remain elusive. Recent research utilizing stable isotope analysis indicates that $\delta^{18}O$ and $\delta^{2}H$ signals in DOM show significant short-term variability during extreme precipitation events, in contrast to stable $\delta^{13}C$ values, which are typical of the terrestrial biosphere. These findings suggested that water isotopes in DOM are potentially informative of DOM transport and turnover. Therefore, to better understand the inland DOM fluxes, the water isotopic ($\delta^{18}O$ & $\delta^{2}H$) and carbon isotopic ($\delta^{13}C$) composition of three DOM components as well as the chromophoric properties of DOM in the pristine Plešné lake were investigated in this thesis. The methodology involved sampling from four different sampling sites, filtering, fractionating DOM into three components via solid phase extraction, excitation emission fluorescence, and analysis via isotope ratio mass spectrometry. The analysis revealed that $\delta^{2}H$ and $\delta^{18}O$ signals in DOM showed greater variability than $\delta^{13}C$ signals, with the SPE-DOM fraction showing the highest stability in isotopic composition and highest reproducibility. A correlation was observed between the $\delta^{2}H$ signal and the fluorescence index as well as the biological index. These trends were followed the strongest by the SPE-DOM fraction. These findings may be used as a baseline for further investigations exploring the relations between $\delta^{2}H$ and fluorescent indices in other watersheds.

Table of contents

List of used abbreviations and symbols

%C: Weight percentage of carbon

°C: Degree Celsius

µL: microlitres

µm: micrometre

BIX: Biological Index

CO: Carbon monoxide

CO_2: Carbon dioxide

DOC: Dissolved Organic Carbon

DOM: Dissolved Organic Matter

EEM: Excitation Emission Matrix

FI: Fluorescence Index

GISP: Greenland Ice Sheet Precipitation

GMWL: Global Meteoric Water Line

H: Hydrogen

H_2: Hydrogen gas

H_n: non-exchangeable Hydrogen

H_2O: Water

HCl: Hydrochloric acid

He: Helium

HIX: Humification Index

IAEA: Internation Atomic Energy Agency

IRMS: Isotope Ratio Mass Spectrometry

L: Litre

mg: milligram

mg L^{-1}: milligram per Litre

min: minute

mL: millilitres

mL min^{-1}: millilitres per minute

N_2: Nitrogen gas

NaOH: Sodium Hydroxide

O: Oxygen

O_n: non-exchangeable Oxygen

Pg: Petagram

Pg C: Petagram Carbon

PL: Plešné

Pl 1: Plešné inlet tributary

Pl dno: Plešné deep water

PL HL: Plešné surface water

PL VY: Plešné exit tributary

SHA: Slightly Hydrophobic Acid

SPE: Solid Phase Extraction

SPE-DOM: DOM extracted via PPL cartridges

USGS: United States Geological Survey

VHA: Very Hydrophobic Acid

VSMOW: Vienna Standard Mean Ocean Water

α: Isotopic fractionation factor

δ: Delta Value

1. Introduction

1.1 Dissolved organic matter

1.1.1 Definition and Importance of DOM

Various forms of organic matter, including ions, colloids, particles, and dissolved molecules, can be found in water. This thesis focuses on dissolved organic matter (DOM), which is operationally defined as the fraction of organic matter found in water samples filtered with a 0.45 µm filter (Perdue & Richie, 2003). Organic material can enter the aqueous system in a variety of ways, and depending on how it enters, DOM can be classified differently and has different properties. Most of the DOM in inland waters is of terrestrial origin, this is known as allochthonous DOM. DOM produced by photosynthetic organisms in the water is known as autochthonous DOM, while DOM originating from human sources is called anthropogenic DOM (Vogt et al., 2023). DOM, independently of its origin, has been investigated since the early 1900s and the interest in it as a research topic has been increasing exponentially since then (Perdue & Richie, 2003).

In face of the changing climate, the global carbon cycle has been investigated from many different perspectives in the last decades. One component of the global carbon cycle, which remains challenging to understand, is the transfer of terrestrial carbon to the open oceans along the aquatic continuum. This transfer is heavily influenced by DOM which makes up to 55% of the total carbon transported (Bauer et al., 2013; Regnier et al., 2013; Ludwig et al., 1996). The importance of DOM is not solely constricted to the carbon cycle, as DOM is an essential source of energy and carbon for aquatic microbes in both marine and freshwaters. The extent of DOM as an energy and carbon source can be seen in humic lakes, where DOM is able to support the growth of zooplankton even in the absence of primary production (Tranvik, 1992; Salonen & Hammar, 1986). DOM may not only be a source of carbon for aquatic organisms, but it can also be a source of biologically available phosphorus rich and nitrogen rich compounds. The nitrogen rich compounds, in the form of ammonium and amino acids, may be secreted from lysed cells or photoproducts formed via photodegradation of humics under UV light. Phosphorus rich substances, in the form of phosphate, may additionally be released from iron complexes, which consist of bound phosphate and humic substances, via reduction driven by UV light (Bushaw et al., 1996; Francko & Heath, 1982). Therefore, DOM is a vital component when one wants to understand the ecology of aqueous ecosystems or the global carbon cycle. Studying DOM fluxes and fates is challenging as its composition, chemical properties and concentration are influenced by its source and can vary

greatly (Leenheer & Croué, 2003). Therefore, researchers have devised several approaches to investigate the different sources and cycling of DOM.

1.1.2 Excitation Emission Matrix and DOM Origin

To investigate organic matter in aquatic environments, fluorescence has been utilized extensively in the last 70 years in water science. Fluorescence describes a phenomenon that occurs when an excited electron returns to its ground state and its lost energy is emitted as light. The excited state is reached when a weakly bound electron absorbs energy, which can occur via the absorption of a photon, and thereby enters a higher energetical level. As a weakly held electron is needed for fluorescence not every organic molecule is therefore capable of it. Hence, in DOM the most studied components via fluorescence include humic substances, which are composed of humins, humic acids, and fulvic acids, and amino acids found in peptides and proteins (Hudson et al., 2007). A special fluorescent technique is called Excitation Emission Matrix (EEM) whereby across a range of wavelengths the intensity of excitation, emission, and fluorescence are scanned synchronously and plotted on a single figure, called the Excitation Emission Matrix (Hudson et al., 2007). The EEMs are used for further assessment of DOM spectroscopic characteristics and allow to determine three indices namely: the humification index (HIX), the biological index (BIX), and the fluorescence index (FI). These indices can be utilized as tracers to investigate DOM sources and transformations. The HIX is a measure for the relative extent of humification. While humification remains poorly defined, it has been described by Flores (2014) as the relative oxidation of organic material. Using this definition, high HIX values may indicate a high degree of oxidation, while low values show a low degree of oxidation of the organic material. The BIX gives a measure for recent autochthonous contribution to the DOM pool, where high values correspond to autochthonous DOM and low values indicate allochthonous DOM. The FI allows to differentiate between fulvic acids of terrestrial origin (allochthonous DOM) and fulvic acids derived from microbial activity (autochthonous DOM), whereby lower FI values correspond to DOM of terrestrial sources, while higher values correspond to DOM of microbial sources, thereby allowing to distinguish DOM based on its different sources (Vogt et al., 2023; McKnight et al., 2001; Xu et al., 2021; Flores, 2014). Given that DOM consists of a complex mixture of various molecules from different sources, fractionating it into different components promotes a more detailed investigation. This fractionation will be discussed in the next part of the introduction.

1.1.3 Fractionation of DOM

One of the earliest studies of DOM in freshwaters was conducted in 1957 by Joseph Shapiro. In this study, one fraction of DOM was isolated from lake water via ethyl acetate extraction and tested in a variety of ways. One of the main conclusions from this research was, that the yellow colouring component of DOM is entirely composed of carboxylic acids (Shapiro, 1957). Since then, DOM has been isolated and fractionated by a wide variety of approaches, such as fractionation by size, via membranes through reverse osmosis followed by ultrafiltration, and by adsorbing onto different resins (a.k.a. solid phase extraction, SPE). These techniques, fractionate DOM by molecular weight and chemical properties, such as acidity and polarity, respectively. (Leenheer, 1981; Crum et al., 1996). A commonly used approach follows the SPE method published by Leenheer (1981), this setup uses three resins and fractions DOM into six parts. The fractions are hydrophobic bases, hydrophobic acids, and hydrophobic neutrals, all these fractions are adsorbed by the XAD-8 resin and eluted via different methods. The hydrophilic bases are adsorbed by the AG-MP-50 resin, hydrophilic acids are adsorbed by the Duolite^{TM} A-7 resin, and the hydrophilic neutrals are extracted via freeze concentration. The mean proportional contributions of these six fractions to the dissolved organic carbon (DOC) are depicted in Figure 1.

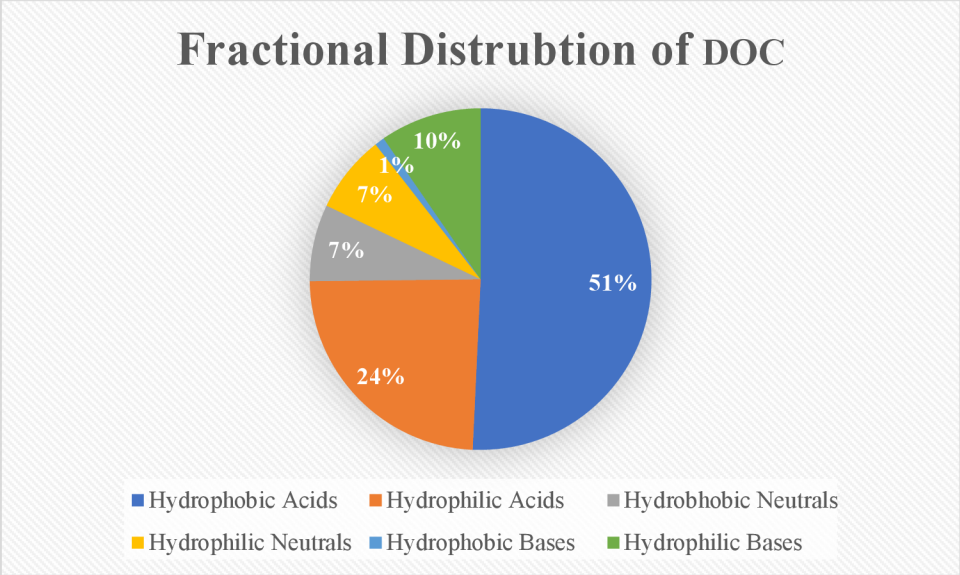

Fig. 1: Shows the contribution of the six fractions defined by Leenheer (1981) to the total dissolved organic carbon. Data taken from Perdue & Ritchie (2003).

Figure 1 shows that within the composition of DOC, dissolved acids, especially the hydrophobic acids, make up the major fraction of it, while the hydrophilic and hydrophobic bases constitute only for a minor fraction of DOC. The average DOM fractions in Lake Plešné, the target site investigated in this thesis, also conform to this trend. This has been investigated by Porcal et al. (2004) for the

hydrological year 2001. Porcal found that acids constitute 74%, 58% hydrophobic and 16% hydrophilic, neutrals 19%, hydrophobic 5% and hydrophilic 14%, and bases 7% of the average DOM isolated from Lake Plešné. Therefore, to better analyse the acidic portion of DOM, multiple procedures based on Leenheer have been developed. One procedure which fractions DOM into 4 parts using 3 resins has been described by Chow et al. (2004). The fractions are very hydrophobic acids (VHA) adsorbed by Supelite™ DAX-8 resin, slightly hydrophobic acids (SHA) adsorbed by Amberlite™ XAD-4 resin, hydrophilic charged fraction adsorbed by Amberlite™ IRA-958, and a hydrophilic neutral fraction which is isolated from the leftover eluent.

Another common SPE approach to extract DOM from water was described by Dittmar et al. in 2008. This method uses commercially available cartridges, usually PPL, to extract DOM via a simple, robust, and efficient method. The extracted DOM is selected by the resin according to its chemical properties and represents a specific component of DOM termed SPE-DOM in this thesis. The biggest advantage of this method is the high extraction efficiency, up to 65% of DOC from river and marsh waters, of desalted DOM, while employing a fast and relatively non-laborious protocol (Dittmar et al., 2008). Due to the different fractionation and extraction methods, DOM can be investigated in a great variety of ways, as discussed below.

1.1.4 DOM fluxes and the Global Carbon cycle

DOM is a complex mixture composed of a wide variety of different molecules with different chemical and physical properties. Therefore, DOM has been studied and characterized in many ways, including the acid-base chemistry, photochemistry, complexation of trace metal cations, bioavailability, and the associated quantitative fluxes. To describe all the different methods by which DOM has been analysed would go beyond the scope of this thesis, therefore this section only focuses on the analysis of DOM fluxes, which are among the most relevant in terms of contributions of DOM to environmental and ecological cycles.

DOM fluxes describe the rate at which DOM moves between reservoirs. The reservoirs in question can vary depending on the model from big reservoirs, such as continents and oceans when looking at global nutrient cycles, to smaller reservoirs, for instance lakes when investigating local carbon budgets (Stets et al., 2009; Regnier et al., 2013). The global carbon cycle depicts all the fluxes of carbon between its different reservoirs, with the major ones being the atmosphere, the oceans, terrestrial land (sometimes also called biosphere), and the lithosphere. Their respective carbon storage for the oceans, biosphere and atmosphere are 38 000 Pg, 2 000 Pg, and 730 Pg. The lithosphere is the biggest reservoir of carbon but mostly inactive, meanwhile the other three carbon

pools are active and tightly coupled (Malhi, 2002; Ussiri et al., 2017). This is shown by the flux of carbon between the ocean and biosphere, here each year up to 2.9 peta-gram (Pg) of carbon from mostly terrestrial origin enter the inland waters and a significant part of it, up to 1 Pg C, is shuttled into the open ocean via rivers (Regnier et al., 2013). This transfer of carbon from land to sea has important consequences for the distribution of carbon between atmospheric, aquatic, and sedimentary reservoirs (Regnier et al., 2013). The land-ocean aquatic continuum does not solely shuttle carbon, it can be considered the zone where nutrients are affected and transformed by a sequence of physic-chemical and biogeochemical processes during their transit from uplands to the oceans (Bouwman et al., 2013). Therefore, the aquatic continuum from inland ecosystems to the oceans has been heavily investigated (e.g., Sarmiento & Sundquist, 1992).

Lateral transfer of carbon, which was thought to remain unaffected by anthropogenic influences, has been neglected in the past anthropogenic carbon dioxide budget reports, such as reports released by institutions like the Global Carbon Project (Regnier et al., 2013). Although, recent evidence suggests that lateral transfer of carbon is affected by anthropogenic influences with estimates as high as 1 Pg C per year. About 50% of the anthropogenic carbon delivered to the aquatic continuum remains sequestered in inland waterbodies and in coastal and estuarine sediments, thereby influencing the distribution of carbon between atmospheric, aquatic, and sedimentary reservoirs. In face of the changing climate and hydrological cycles, DOM fluxes are expected to change and increase in the future. Thus, correct assessment of inland carbon fluxes, and thereby bettering our understanding of lateral carbon fluxes, is vital (Bauer et al., 2013; Regnier et al., 2013; Raymond & Spencer, 2015).

For the lateral transport of terrestrial matter, two fluxes are of importance: the introduction of DOM of terrestrial origin to inland waters and the subsequent transfer of riverine and terrestrial DOM to the oceans (Raymond & Spencer, 2015). To grasp the dynamics of inland carbon fluxes and in extension DOM fluxes, it becomes vital to understand the various pathways through which carbon is introduced. Two major pathways are responsible for the introduction of over 90% of the carbon to inland waters. The first pathway describes the export of inorganic carbon of terrestrial origin, which includes carbon from soil respiration, chemical weathering, and mechanical weathering. The second pathway describes export of terrestrial organic carbon (Drake et al., 2018; Regnier et al., 2013).

The different sources and transformations of DOM imprint a distinct isotopic footprint, which was used by many studies to investigate the sources and changes of DOM (e.g., Zhang et al. 2020; Pilecky et al., 2023). In this thesis stable isotopes are used to provide insight into previously hidden

fluxes of DOM. The next section of the introduction covers what stable isotopes are, what isotopic fractionation is, and how they can help us detect hidden fluxes.

1.2 Stable Isotopes

1.2.1 General Information

Isotopes are atoms characterized by having an identical number of protons in their nuclei but a varying number of neutrons. Depending on their stability, isotopes can be divided into two categories, stable and unstable (also called radioactive) isotopes. Radioactive isotopes are defined as isotopes that can undergo radioactive decay, while stable isotopes do not undergo radioactive decay (Hoefs, 2015).

Not all isotopes of an element, no matter if stable or unstable, are present in equal amounts. The amount at which a respective isotope is present in an element is given by its isotopic abundance, which can be regarded as the molar fraction of this respective isotope. The isotopic abundance varies among elements, ranging from significant disparities in isotopes, such as Helium with ^{3}He (0.000137%) and ^{4}He (99.999863%), respectively, to nearly equal distributions as observed in Bromine with ^{79}Br (50.69%) and ^{81}Br (49.31%), respectively (Coplen et al., 2002; Rosman & Taylor, 1999). Hydrogen, Carbon and Oxygen, the major components of DOM, exhibit similar isotopic abundancies, with each possessing at least two stable isotopes, with significant disparities like Helium. For instance, Carbon and Hydrogen each possess two stable isotopes, with their respective abundance of ^{1}H (99.9885%) and ^{2}H (0.0115%) for Hydrogen and ^{12}C (98.93%) and ^{13}C (1.07%) for Carbon. While Oxygen comprises three stable isotopes, with their respective abundance of ^{16}O (99.757%), ^{17}O (0.038%), and ^{18}O (0.205%) (Perdue & Richie, 2003; Rosman & Taylor, 1999).

The different number of neutrons in the nuclei is not the sole distinction between stable isotopes of an element. Due to their different atomic mass, a difference in chemical and physical properties arises. The differing physical properties can be observed well on the example of water. For example, normal water $^{1}H_2{}^{16}O$ has a density of 0.997 g cm^{-3} at 20 °C, with its temperature of greatest density occurring at 3.98 °C. In contrast, $^{2}H_2{}^{16}O$ and $^{1}H_2{}^{18}O$ has a density of 1.1051 g cm^{-3} and 1.1106 g cm^{-3} at 20 °C as well as a temperature of greatest density of 11.24 °C and 4.30 °C, respectively (Hoefs, 2015).

The different properties of the isotopes have many consequences, such as those that give rise to the global meteoric water line (GMWL). The GMWL characterises how global trends in evaporation and precipitation fluxes systematically distribute Oxygen and Hydrogen isotopes in naturally

occurring meteoric waters. Accordingly, the ratios of both $^{2/1}H$ and $^{18/16}O$ in meteoric water follows a simple linear relationship, shown in Equation 1 (Craig, 1961; see Section 1.2.2 for explanation of delta notation).

$$\delta^2H = 8 * \delta^{18}O + 10 \qquad \textbf{Eq. 1}$$

Via the GMWL, the relationship between the $\delta^{18}O$ and δ^2H values can be predicted reliably in precipitation. Although the relationship between ^{18}O and ^2H remains unchanged, precipitation displays a varying isotopic signal. Whereby a higher fraction of heavier isotopes is found in rainfall near the oceans than in rainfall on the continental interiors (Ehleringer et al., 2008). Due to this a spatial distribution of hydrogen and oxygen isotopes in waters can be expected. Such a map of the world with the differing hydrogen isotopes can be seen in Figure 2.

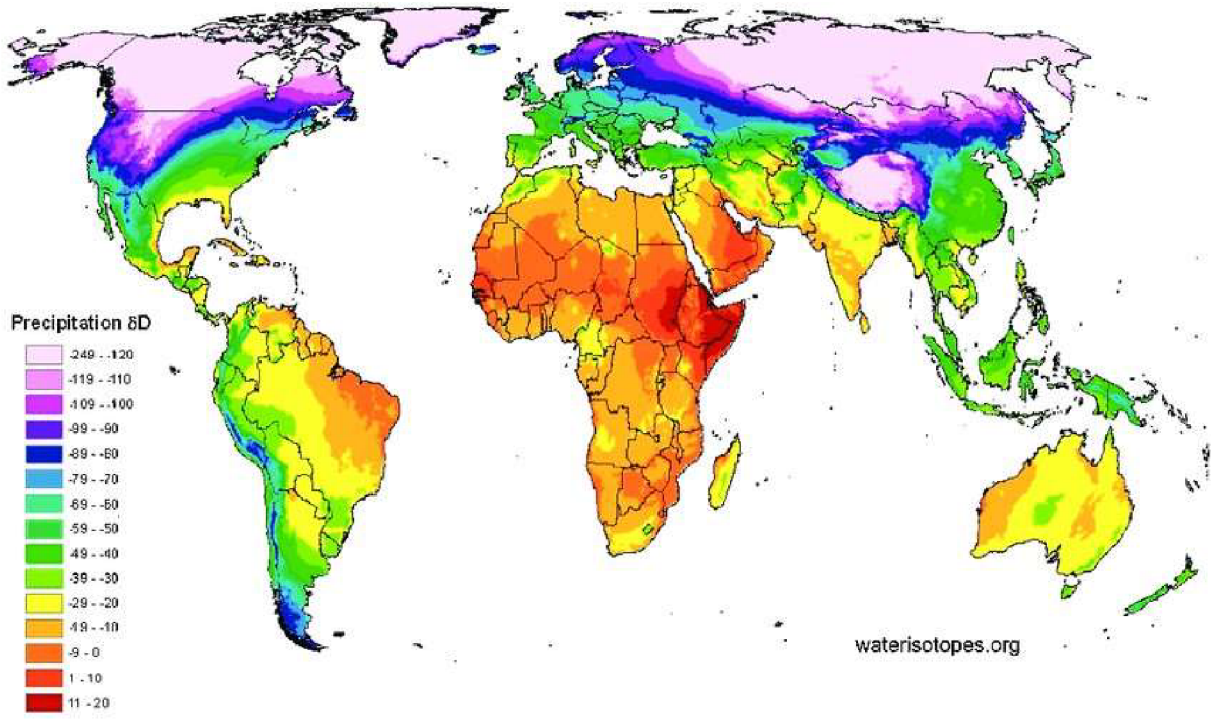

Figure 2: Predicted average yearly precipitation hydrogen isotope ratios. Prediction is based in combination of empirical relationship between measured precipitation, latitude, and elevation. For unexplained regions a geostatistical smoothing algorithm was used, according to Ehleringer et al. 2008.

Due to this spatial distribution one can make predictions about the origin of meteoric water based on its isotopic composition. But not only physical processes are altered by the different atomic masses of the isotopes, also physical-chemical properties are affected by it (Hoefs, 2015). These

slight alterations may be the window to uncover the hidden fluxes of DOM. How and which processes are altered are discussed in the next part of the introduction.

1.2.2 Isotopic Fractionation

While the nucleus mainly dictates physical properties, the electrons mainly determine the chemical properties of an atom. From this one would expect identical chemical properties between the isotopes of an element. But there also exist, albeit small, differing physical-chemical properties between different isotopes of an element.

The changed physical-chemical behaviour is manifested in altered kinetic processes and exchange rates. Consequently, this results in varying relative isotope abundances within two phases or substances composed of the same material, this phenomenon is called "isotopic fractionation" (Hoefs, 2015).

Isotopic fractionation processes can be found in a wide range of disciplines ranging from Hydrology, due to GMWL, to Botany, due to different ^{13}C signal in C_3 and C_4 plants (Hoefs, 2015). Therefore, understanding and measuring the isotopic signals can be a potent analytical tool for examining the origin of substances or better understanding fluxes (e.g., Ye et al., 2018; van Heemst et al., 2000).

To use the disparity in isotopic composition, emerged via isotopic fractionation, to its fullest potential, the findings about the stable isotope ratios must be quantified. To quantify these findings two concepts, namely the delta notation (δ) and the isotopic fractionation factor alpha (α) must be introduced. The delta notation is used to report composition of stable isotopes. The values are reported as per mill (‰) deviations of the measured material in relation to a known standard as seen in Equation 2 (Kendall & Caldwell, 1998).

$$\delta(in\ ‰) = \left(\frac{R_x}{R_s} - 1\right) \cdot 1000 \qquad \textbf{Eq. 2}$$

R_x Ratio of heavy to light isotope in the sample

R_s Ratio of heavy to light isotope in the standard

While the delta value depicts the isotopic composition of a substance, the alpha value refers to the extent of isotopic fractionation (difference in isotopic composition) between any two phases as seen in Equation 3 (Sharp, 2017). The isotopic fractionation factor heavily depends on temperature, with fractionation reaching 0 at very high temperatures (Hoefs, 2015).

$$\alpha_{A-B} = \frac{1000 + \delta_A}{1000 + \delta_B} \qquad \textbf{Eq. 3}$$

The equation above gives a measurement of the enrichment or depletion of a certain isotope of A compared to B, an alpha value > 1 indicates an enrichment while < 1 indicates a depletion. The enrichment and depletion of isotopes accumulated during the lifetime of molecules can be measured and used to determine the origin and fluxes of DOM, how this is done is shown in the next chapter.

1.2.3 Isotopic Fractionation of DOM

DOM is mainly composed of hydrogen, carbon, and oxygen, therefore isotopic fractionation processes of these elements are of particular interest for this thesis.

Carbon is incorporated into organic matter via photosynthesis. During photosynthesis plants can more easily (rapidly) incorporate the lighter ^{12}C isotope than the heavier ^{13}C isotope, therefore effectively discriminating against ^{13}C. But not all plants show the same discrimination, as the fractionation taking place is unique to the plant's environmental factors and metabolism. The most striking difference can be found between the different plant metabolisms, whereby C_3 plants, which contain CO_2 via the carboxylation of the enzyme ribulose biphosphate, show mean $\delta^{13}C$ values of -28.1‰ ± 2.5‰. While C_4 plants, which bind CO_2 via phosphoenolpyruvate, incorporate more ^{13}C with mean $\delta^{13}C$ values of -13.5‰ ± 2.5‰. The special case of crassulacean acid metabolism (CAM) plants employ both the C_3 and C_4 metabolism depending on illumination, and therefore show $\delta^{13}C$ values ranging from -13‰ to -27‰. In addition to the metabolism, environmental factors such as temperature, light intensity, CO_2 source, and habitat influence fractionation (O'Leary, 1981).

Not only carbon is incorporated into biomass during photosynthesis, but also hydrogen and oxygen. For these two elements, there are two types of biological processes which can influence the isotopic fractionations, namely fractionation during biosynthesis of cellulose and evaporative transpiration of leaf water (DeNiro & Epstein, 1981). Unlike carbon, hydrogen experiences a wide range of observed δ^2H values emerging during biosynthesis ranging from -400‰ to +200‰, these values can vary greatly between different species grown in the same environment and depend on factors such as temperature and water availability (Hoefs, 2015; DeNiro & Epstein, 1981). For oxygen, the isotopic fractionation does not show such big ranges; cellulose found in organisms shows $\delta^{18}O$

values of 27‰ ± 3‰ compared its source water, which yields an isotopic fractionation factor of ^{18}O $\alpha_{Cellulose\text{-}Water}$ of 1.027 ± 0.003. (DeNiro & Epstein, 1981).

Hydrogen can bind in organic matter either to carbon, thereby being unsusceptible to equilibrium exchange reactions, or bind to heteroatoms (O, S, N). The latter group being able to exchange its hydrogen freely and uncontrollably with ambient water or water vapor. To determine the intrinsic isotopic signal of non-exchangeable hydrogen (H_n), which is derived from its local water environment at the moment of biosynthesis, special methods, such as the dual vapour equilibration, were developed (Wassenaar et al., 2023). The intrinsic hydrogen signal may then be useful to trace the organic material to its source (e.g., similarly to GMWL interpretations), while the exchangeable hydrogen fraction tells us something about the chemical composition of the organic material. This novel approach is parallel to ^{13}C analysis, which has been demonstrated to be a potent tool for analysing organic material and thereby gaining information about DOM fluxes (e.g., Meador & Aluwihare, 2014).

However, a recent study by Pilecky et al. (2023) showed that C isotope signal from DOM from a subalpine lake system is not sufficiently variable in short-time periods under extreme precipitation events to identify input of allochthonous carbon. This research also showed that, in contrast, large isotopic fluctuations are recorded in δ^2H_n and $\delta^{18}O$ from DOM, which suggested DOM relocation and turnover. This opens a venue to using isotope ratios of both δ^2H and $\delta^{18}O$ from DOM as a record of fluctuations on local hydrological conditions to advance the study of organic C cycling in inland waterbodies and thus, the land-ocean aquatic continuum. This thesis was conducted as part of a bigger project focused around the hydrogen and oxygen isotopes and cycling of humics in peat and sought to fractionate DOM into SPE-DOM, SHA, and VHA and subsequently analyse these fractions via the dual vapour equilibration method to better understand these hidden fluxes shown via δ^2H_n and $\delta^{18}O_n$ values.

2 Thesis Aims

This thesis aims to investigate the water isotopic (δ^2H and $\delta^{18}O$) and carbon isotopic ($\delta^{13}C$) composition of three DOM fractions isolated from four sampling sites in the acidified glacial lake Plešné, located in the Šumava National Park, to better our understanding of inland DOM fluxes. To achieve this aim, seasonal signals mirrored in the dissolved organic carbon and DOM concentrations and the chromophore properties of the water samples are additionally investigated.

3 Methods

3.1 Materials

All essential equipment, chemicals, and international standards used during the experiment are listed below.

3.1.1 Equipment

The used equipment is listed below:

- 2.7 µm pore size GF/D and 0.4 µm pore size MN GF-5 glass fibre filter
- Glass vials (2mL, 15 mL) and glass test tubes (10 mL)
- Variable-volume micro and macro pipettes with disposable plastic tips (100 µL, 1000 µL, 5mL, 10 mL)
- Silver and tin capsules
- ECP2011 Analytical Single-Piston Pump
- 2x Diba Omnifit® EZ SolventPlus™ Chromatography Column with 2 Fixed Endpieces (25 mm ID x 150 mm L)
- Supelite™ DAX-8, Amberlite™ XAD-4, and AmberChrom™ (H+) Cation Exchange resin
- Bond Elut PPL cartridges (100mg bed mass, 3 mL volume)
- VacElut Cartridge Manifold and 12x Bond Elut Adapters
- Fume hood and personal safety equipment

3.1.2 Reagents and reference materials

The used reagents are listed below together with its producer:

- Methanol (>99.8%, Sigma-Aldrich)
- Milli-Q® water (Sigma-Aldrich)
- HCl (37%, Sigma-Aldrich)
- NaOH (Sigma-Aldrich)
- He gas (Messer)
- Ar gas (Messer)
- Qlarivia 15 and GFLES-4 water standards

3.1.3 International Standards

The laboratory standards used to determine isotope composition of organics are listed below. International reference material standards (shown below in *italics*) were provided by the International Atomic Energy Agency (IAEA) and United States Geological Survey (USGS) and are used to normalize the measured isotope ratios of C, H, and O to the internationally accepted reference scales.

For carbon, a variety of international and in-house standards are used, including:

- Mate -30.1‰
- *Caffeine* (IAEA-600) -27.77‰
- Peat -28.1‰
- Fish muscle -25.5‰

Hydrogen and Oxygen isotope composition of international reference materials (respectively) included:

- *Vienna Standard Mean Ocean Water (VSMOW)* 0.0‰ 0.0‰
- *Greenland Ice Sheet Precipitation (GISP)* -189.7‰ -24.8‰
- *UC04-15* 113.6 ‰ 39.0‰

3.2 Sampling Site

To achieve the goals of the thesis, water samples (1.0 – 2.0 L) were collected from a water body located in the South Bohemia Forest landscape. Plešné Lake (PL) is an acidified glacial lake with a surface area of 7.5 ha with maximum depth of 18 m that is found at 1090 m above sea level at the Šumava Mountains (48°47´N, 13°52´E; Porcal et al. 2004). PL catchment is enclosed by a regrowing conifer forest comprising the strictly protected area of the Šumava National Park, and thus, anthropogenic effects are minimal (Vystavna et al. 2021). Water samples were collected from 4 different sites, PL-VY, the exit tributary, PL-1, inlet tributary, PL-dno, deeper part of the lake at 17 m, and PL-HL, lake surface. Sample collection was performed by routine sampling excursion by the Institute of Hydrobiology of the Biology Centre of the Academy of Sciences at three-week intervals from May until December 2022. Samples were collected in 2L pre-washed polyethylene terephthalate (PET) containers and ultimately filtered through 0.4 µm MN GF-5 glass fibre filter, then stored at 4 °C until further processing.

3.3 Sample preparation

The filtered water samples were divided into multiple fractions for the different extraction methods and stored in the fridge for subsequent analysis. A methodological scheme is detailed in Figure 3.

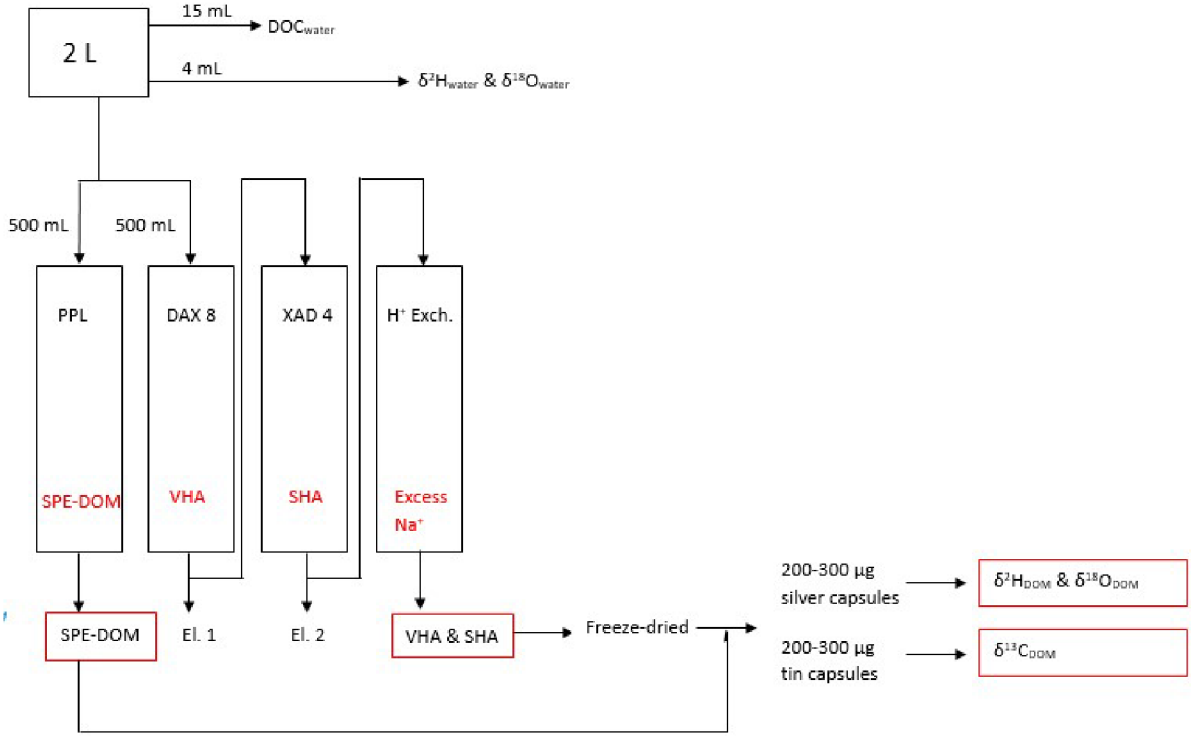

Figure 3: Graphical schematic of the followed methodological approach.

3.4 DOC Measurement

To monitor the DOC content of the samples, aliquots were taken after sample preparation as well as before and after the neutralisation during column extraction. The DOC analysis was performed by Petr Porcal's research group at the Institute of Hydrobiology of the Biology Centre of the Academy of Sciences, according to the method described in Porcal et al. (2004).

3.5 Column Extraction with DAX-8 and XAD-4 resins

To fractionate DOM into very hydrophobic acids (VHA) and slightly hydrophobic acids (SHA), two different resins were used for solid phase extraction. The fractionation setup was based on the method described by Chow et al. (2004) and resulted in two fractions: VHA absorbed by the Supelite™ DAX-8 resin and SHA absorbed by the Amberlite™ XAD-4 resin (Sigma-Aldrich). The filtered water samples were acidified to pH 2 and subsequently filtered again through a 2.7 µm

GF/D glass fibre filter and 0.4 µm MN GF-5 glass fibre filter. For the extraction, a bed height of 5 cm was used for the Supelite™ DAX-8 and Amberlite™ XAD-4 resin, which led to a bed volume of 24.5 ml. Aliquots for DOC measurement were taken before the extraction and after the neutralisation step. The column extraction consisted of 3 steps.

I) Cleaning and activation of the resins:

To clean and activate the resins, the two columns were connected to each other via Teflon tubing to form a DAX-8 & XAD-4 setup and flushed with reagents following the procedure outlined in Table 1.

Table 1: Activation and Cleaning of DAX-8 and XAD-4 resins

Reagent	**Volume**	**Flowrate**
0.1 M NaOH	50 ml	5 ml/min
Milli-Q Water	50 ml	5 ml/min
0.1 M HCl	50 ml	5 ml/min
Milli-Q Water	150 ml	5 ml/min

II) Extraction of VHA and SHA:

To extract the VHA and SHA, the water sample was pushed through the connected DAX-8 & XAD-4 setup using a gear pump at a rate of 5 mL min^{-1}. Afterwards, the two columns were disconnected and the respective VHA and SHA fractions were retrieved via the elution with 0.1 M NaOH and collected in two respective glass bottles. The reagents were passed through the columns according to Table 2.

Table 2: Extraction of VHA and SHA

Reagent	**Volume**	**Flowrate**	**Purpose**
Acidified Sample (pH ≈ 2.0)	500 ml	5 ml/min	Sample Loading
Acidified Milli-Q Water (pH ≈ 3.95)	50 ml	5 ml/min	Pushing Sample through Resins (in series)
0.1 M NaOH	50 ml	2 ml/min	DAX-8 Elution
0.1 M NaOH	50 ml	2 ml/min	XAD-4 Elution

III) Neutralisation of the eluted VHA and SHA via H+ ion exchange resin:

To remove salts formed during the extraction and elution of VHA and SHA, the eluents were passed through a column containing AmberChrom™ (H+) Cation Exchange resin (Sigma-Aldrich). The bed height of the ion exchange resin was 3 cm, which led to a bed volume of 14.7 ml. The

neutralised SHA and VHA samples were collected in round bottom flasks and, to calculate the final volume of the neutralised sample, the round bottom flask was weighed before and after the neutralisation. The reagents were passed through the columns according to Table 3.

Table 3: Neutralisation of VHA and SHA eluents via H+ exchange resin

Reagent	**Volume**	**Flowrate**	**Purpose**
0.1 M HCl	50 ml	5 ml/min	Resin Equilibration
Milli-Q Water	50 ml	5 ml/min	Pushing HCL through resin
DAX-8 / XAD-4 Eluents	50 ml	5 ml/min	Removing Sodium from sample
Milli-Q Water	30 ml	5 ml/min	Pushing Sample through resin

The neutralised VHA and SHA eluents were lyophilized to a dry powder and stored in a desiccator until further analysis.

3.6 DOM extraction with PPL cartridge (SPE-DOM)

Agilent Bond Elut PPL cartridges were also used to extract DOM from sample waters; for the purpose of this thesis, DOM extracted with this method is referred to as SPE-DOM. The method used was based on the procedure described by Dittmar et al. 2008. The filtered water samples (500 mL) were acidified to pH 2. Then the cartridges were connected to a VacElut Cartridge Manifold using Bond Elut Adapters and not used cartridge places were sealed using small caps. Then the cartridges were cleaned with 4 mL methanol followed by 2 mL 0.01 M HCl. When working with the cartridges, it was important to never let the cartridges get dry after one starts with the first cleaning step until all the sample was passed through the cartridges. After the cleaning step the vacuum was turned on and a small funnel was connected to the cartridges. Then 500 mL of the water sample was passed through the cartridges. After this, the cartridges were rinsed with 8 mL 0.01 M HCl to get rid of potential salts. Then the cartridges were left to dry under vacuum conditions. Once the cartridges were dry, the vacuum was turned off, test tubes were labelled accordingly, and placed via a test tube rack under the cartridges. Then the SPE-DOM was eluted from the cartridges using 8 mL methanol. The methanol eluent was then dried under an Argon stream at 35 °C and afterwards stored in the freezer. Afterwards 2 mL vials were tared, the now solid SPE-DOM was transferred to these vials. This was done by dissolving the DOM in 1.2 mL methanol and transferring it, followed by drying under an Argon stream at 35 °C and determination of the final weight of the dry SPE-DOM.

3.7 Preparation for stable isotope analysis

To analyse the oxygen and hydrogen isotopic composition, the extracted and dried SPE-DOM, VHA and SHA samples were weighed into silver capsules, folded into little balls to avoid spillage of the samples, and stored in a desiccator until analysis. As we used the dual vapor equilibration described by Wassenaar et al. (2023) for analysing the samples, we prepared 4 folded capsules for each sample, 2 capsules for high equilibration and 2 capsules for low equilibration. For the analysis of carbon isotopes, the extracted and dried SPE-DOM, VHA and SHA samples were weighed into tin capsules, folded into little balls to avoid spillage of the samples, and stored in a desiccator until analysis. The weight analysed depended on the type of sample, for VHA and SPE-DOM 200-300 µg and for SHA 300-400 µg were analysed.

3.8 Analysis of stable isotopic composition of oxygen and hydrogen

To determine the stable isotopic composition of hydrogen and oxygen, $\delta^{18}O$ and $\delta^{2}H$, the samples were analysed by using a Flash CNSOH Elemental Analyzer interfaced with a MAT253 Plus isotope ratio mass spectrometer (IRMS) via a ConfloIV interface (Thermo Scientific, Bremen Germany). With this apparatus, silver capsules were pyrolyzed at 1400 °C inside a glassy carbon reactor to convert H to H_2 gas and O to CO gas. Helium was used as the carrier gas at 80 mL min^{-1} flow rate, and the resulting gases passed through a magnesium perchlorate trap to remove water and other impurities. Afterwards, gases were further separated at 60 °C on a 1 m Moleseive 5A column. H_2 and CO flowed through a TCD detector for bulk property detection, afterwards the gases flow through the open split and the instrument's ion source. H isotopic composition was calculated based on the ratio of m/z=2 ($^{1}H^{1}H+$) and m/z=3 ($^{1}H^{2}H+$) ions, after accounting for the contribution of $^{3}He+$. ^{18}O isotopic composition was calculated based on the ratio of m/z=28 ($^{12}C^{16}O$) and m/z=30 ($^{12}C^{18}O$).

3.9 Analysis of exchangeable and non-exchangeable hydrogen and oxygen

To determine the exchangeable and non-exchangeable fraction of hydrogen and oxygen in DOM, dual-vapour equilibration was used. The method consists of the equilibration of the samples under two different water vapour atmospheres with widely contrasting $\delta^{2}H$ and $\delta^{18}O$ isotopic signatures for 30 minutes at 70°C prior to pyrolysis (i.e., Qlarivia 15, -879‰ and -196‰, respectively, vs. GFLES-4, 399‰ and -6‰, respectively). The equilibration was performed inside a UniPrep device

coupled to the high-temperature thermochemical elemental analyser and continuous-flow IRMS under vacuum evacuation and He drying to avoid reabsorption of exchangeable H with ambient water vapour (Wassenaar et al. 2023). For non-exchangeable H and O, δ^2H_n and $\delta^{18}O_n$ values were calculated as seen in Equation 5; while the exchangeable fractions (δ^2H_{ex}, $\delta^{18}O_{ex}$) were obtained from the measu1red δ^2H and $\delta^{18}O$ isotopic difference in the unknown sample after equilibration with the two known and widely differing water vapours as seen in Equation 4. Final isotopic data were normalized against the secondary international reference standards as described in section 3.1.3.

$$f_{ex} = \frac{\delta^2H_{sa-E} - \delta^2H_{sa-D}}{\delta^2H_{w-E} - \delta^2H_{w-D}} \quad \textbf{Eq. 4}$$

δ^2H_{w-E} δ^2H value of the enriched equilibration water

δ^2H_{w-D} δ^2H value of the depleted equilibration water

δ^2H_{sa-E} δ^2H value of the sample equilibrated with the enriched water

δ^2H_{sa-D} δ^2H value of the sample equilibrated with the depleted water

$$\delta^2H_n = \frac{\delta^2H_{sa-D} - f_{ex} \cdot \delta^2H_{w-D}}{1 - f_{ex}} \quad \textbf{Eq. 5}$$

In addition, fractionation factors (α) were calculated according to Equation 6 to evaluate the partitioning of the stable isotopes between the water of PL and their DOM components.

$$\alpha_{2H} = \frac{1000 + \delta^2H_{DOM}}{1000 + \delta^2H_{source\ water}} \quad \textbf{Eq. 6}$$

To corresponding ^{18}O parameters are calculated in the same fashion.

3.10 Analysis of stable carbon composition

To determine the stable isotopic composition of carbon, $\delta^{13}C$, the samples were analysed by using a MAT253 Plus isotope ratio mass spectrometer (IRMS) interfaced with a Flash CNSOH Elemental Analyzer via a ConfloIV interface (Thermo Scientific, Bremen Germany). With this apparatus, tin capsules were pyrolyzed at 1020°C inside a tungsten oxide reactor to convert C to CO_2 gas. For this, a pulse of oxygen is introduced simultaneously with the sample. Helium was used as the carrier

gas (70 mL min^{-1}) and the gases passed through a magnesium perchlorate trap to remove water and other impurities. The gases were then separated using a sulphur separation column, where the temperature is held at 70°C for 550 seconds to separate N_2 from CO_2. The now separated gases flow through a TCD detector for bulk property detection, afterwards the gases flow through the open split and the instrument's ion source. C isotopic composition was calculated based on the ratio of m/z=44 ($^{12}C^{16}O_2$) and m/z=45 ($^{13}C^{16}O_2$), after accounting for the contribution of ^{17}O.

3.11 Excitation Emission Matrixes

To further investigate the origin of the different DOM fractions fluorescence indices, excitation emission matrixes, were employed. The EEM analysis was performed by Petr Porcal in the Institute of Hydrobiology of the Biology Centre of the Academy of Sciences according to the method described in Vogt.et al. (2023).

3.12 Statistical Analysis

The statistical analyses were performed utilizing the standard R library. The version of R used was 4.2.3.

3.13 Outlier Detection

Samples with a weight percentage of carbon (%C) below 20% were deemed outliers as these samples are likely contaminated by salts introduced during the extraction protocol. Samples with high salt content are concerning as they may introduce inaccuracies during IRMS analyses, therefore these samples were neglected for the investigation of stable isotopes. The list of the %C values can be found in the appendix (A4, A5, A6).

4. Results

4.1 DOC and DOM Extractions

To investigate seasonal variability and trends, three different types of DOMs were extracted via two different protocols. Additionally, the total amount of carbon in the water samples was analysed via DOC measurements. In the first part of the result section the findings of the different extraction methods are presented.

4.1.1 DOC and DOM Trends

DOC concentrations as well as the three different types of DOM components are depicted in Table 4. To better compare the three DOM fractions to each other and to minimize the influence of variations in different extraction volumes, the DOM fractions are depicted as % DOC recovered. DOC samples were collected before and after the fractionation and extraction of DOM into VHA and SHA. This allows for the determination of the % DOC recovered, which was determined according to Equation 7. As no DOC samples were collected after the extraction of SPE-DOM, due to the likely traces of methanol remaining from the earlier cleaning step (P. Porcal, personal communication), the % DOC recovered for this fraction was calculated according to Equation 8.

$$\%\, DOC_{VHA\,/\,SHA} = \frac{(DOC_{extracted\ sample} \cdot V_{extracted\ sample})}{(DOC_{inititat} \cdot V_{initial})} \qquad \textbf{Eq. 7}$$

DOC Concentration of dissolved organic carbon / mg L^{-1}

V Volume / L

$$\%\, DOC_{SPE} = \frac{\frac{(m_{SPE} \cdot \%C_{SPE})}{V_{SPE}}}{DOC} \qquad \textbf{Eq. 8}$$

m_{SPE} mass of extracted SPE-DOM component / mg

$\%C_{SPE}$ weight percentage of carbon in the extracted SPE-DOM component / %

Table 4: DOM components and DOC concentrations of the four sampling sites. The DOM components were depicted as %DOC recovered and the samples were collected over a time frame of half a year.

Sampling Site	C_{DOC} / mg C L^{-1}	$\%DOC_{VHA}$ / %	$\%DOC_{SHA}$ / %	$\%DOC_{SPE}$ / %
PL 1 09.05.2022	21.98	90%	44%	43%
PL 1 30.05.2022	18.33	178%	114%	33%
PL 1 22.06.2022	20.40	111%	80%	38%
PL 1 11.07.2022	24.04	74%	54%	35%
PL 1 01.08.2022	22.11	129%	39%	43%
PL 1 22.08.2022	19.22	162%	93%	34%
PL 1 05.09.2022	19.75	73%	85%	42%
PL 1 24.10.2022	20.39	83%	22%	63%
PL 1 05.12.2022	22.28	91%	25%	39%
Mean	17.12	110%	62%	41%
PL dno 09.05.2022	10.29	74%	30%	38%
PL dno 30.05.2022	10.38	60%	28%	65%
PL dno 22.06.2022	10.14	60%	18%	38%
PL dno 11.07.2022	10.43	46%	9%	39%

PL dno 01.08.2022	9.83	62%	10%	36%
PL dno 22.08.2022	10.69	49%	10%	46%
PL dno 05.09.2022	10.50	49%	10%	49%
PL dno 24.10.2022	9.61	50%	23%	56%
PL dno 05.12.2022	10.95	47%	10%	38%
Mean	10.31	55%	17%	45%
PL HL 09.05.2022	9.99	49%	30%	66%
PL HL 30.05.2022	9.94	83%	25%	76%
PL HL 22.06.2022	10.80	53%	17%	29%
PL HL 11.07.2022	12.77	60%	15%	42%
PL HL 01.08.2022	12.68	74%	15%	36%
PL HL 22.08.2022	11.97	60%	8%	30%
PL HL 05.09.2022	11.50	60%	9%	26%
PL HL 24.10.2022	11.04	54%	10%	31%
PL HL 05.12.2022	10.56	72%	12%	28%
Mean	11.25	63%	16%	40%
PL VY 09.05.2022	9.89	68%	11%	54%
PL VY 30.05.2022	10.59	44%	7%	53%
PL VY 22.06.2022	10.89	29%	9%	27%
PL VY 11.07.2022	13.06	50%	10%	40%
PL VY 01.08.2022	12.48	54%	9%	38%
PL VY 22.08.2022	12.09	42%	9%	48%
PL VY 05.09.2022	11.06	66%	27%	32%
PL VY 24.10.2022	10.88	65%	21%	53%
PL VY 05.12.2022	10.65	52%	6%	35%
Mean	11.29	52%	12%	42%

To better investigate the seasonal variability, the DOC and SPE-DOM concentrations were plotted in Figure 4 and 5, respectively. To better compare the different DOM concentrations to each other and to minimize the influence of variations in different extraction volumes, the DOM concentrations are given in mg L^{-1}. These values were obtained by dividing the dry weight, determined via weighing the entire DOM sample by the extraction volume, as seen in Equation 9. The values used for plotting can be found in the Appendix (A1) together with the plotted SHA and VHA components (A2 & A3).

$$C_{DOM} = \frac{m_{DOM}}{V_{DOM}} \qquad \textbf{Eq. 9}$$

C_{DOM} Concentration of DOM / mg L^{-1}

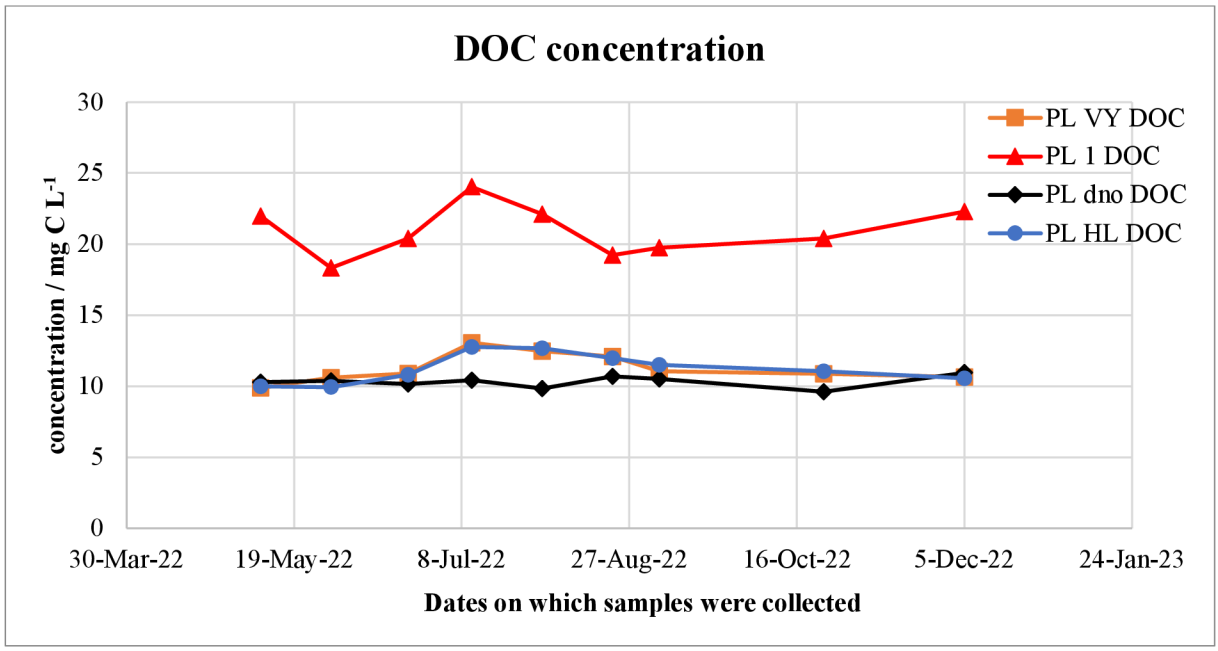

Figure 4: DOC concentration in Lake Plešné. PL 1 is the inlet tributary, PL HL is surface water, PL dno is deep water, and PL VY is the exit tributary.

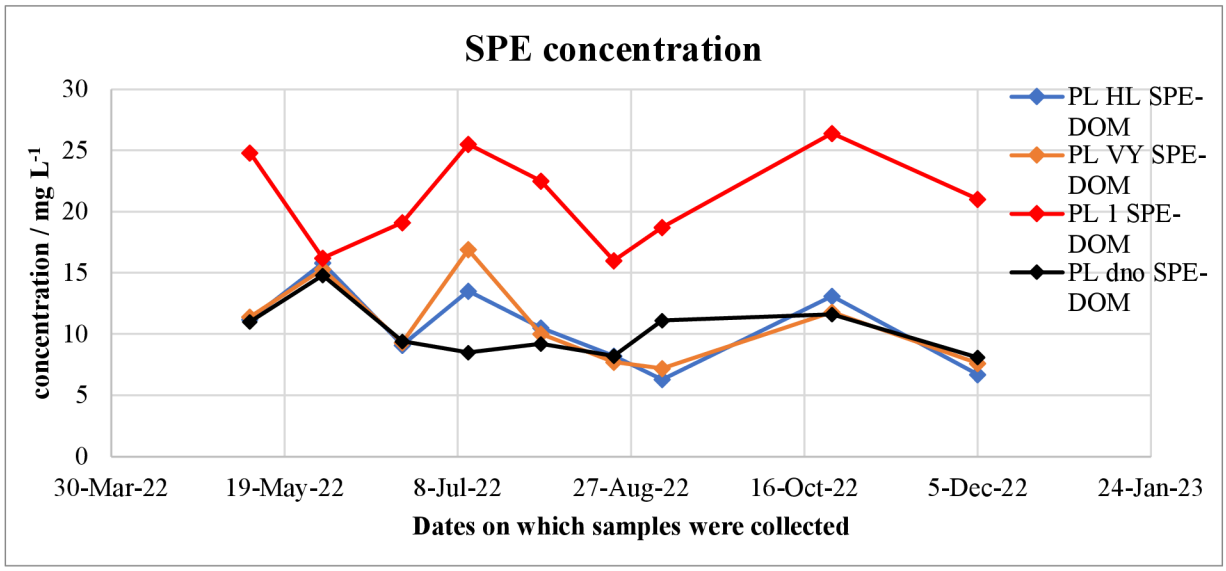

Figure 5: SPE-DOM concentration in Lake Plešné. PL 1 is the inlet tributary, PL HL is surface water, PL dno is deep water, and PL VY is the exit tributary.

Samples collected from the lake's surface (PL-HL) exhibited a concentration range of 10.0 to 12.8 mg L^{-1} and 6.3 to 15.8 mg L^{-1} for the DOC and SPE-DOM concentration, respectively. High DOC values were measured during the summer months, July and August, with the spring and summer samplings showing little variation and values around 10 mg L^{-1}. Both the DOC and SPE-DOM concentrations at PL-HL were similar to the lake's exit tributary (PL-VY). PL VY showed concentration ranges of 9.9 to 13.1 mg L^{-1} and 7.2 to 16.9 mg L^{-1} for the DOC and SPE-DOM

concentration, respectively. PL VY follows the same DOC trend as the surface water. For the SPE-DOM concentration PL VY showed its highest peak at the beginning of the summer followed by a gradual decline in concentration, until the concentration rises again in late fall. The same trend can be observed for the lake's inlet tributary (PL 1) which showed concentration ranges of 18.3 to 24.0 mg L^{-1} and 16.0 to 26.4 mg L^{-1} for the DOC and SPE-DOM concentration, respectively. PL 1 exhibited the highest DOC and SPE-DOM concentration among all sampling sites. With the highest values for DOC again observed in the summer months. The highest SPE-DOM concentration was measured in late fall. The lake's deep water (PL dno) showed the lowest concentrations among all sampling sites, with the exception of the SPE-DOM sample collected on the 05.09.2022, with concentration ranges of 9.6 to 11.0 mg L^{-1} and 8.1 to 14.8 mg L^{-1} for the DOC and SPE-DOM concentration, respectively.

4.2 Isotopic Analysis

The first part of the results section focused on the trends and variations observed between the three DOM fractions and DOC for the different sampling sites. The focus of the following result section lies on the trends and variations of the isotopic signals between different sampling sites and DOM fractions.

4.2.1 Stable carbon, hydrogen, and oxygen isotopes

To investigate the variability of the carbon, hydrogen, and oxygen isotopic composition ($\delta^{13}C$, $\delta^{2}H_n$, and $\delta^{18}O_n$), these values were plotted in Figure 6 and the variability in data was compared to the typical error of measurement. The isotopic values used for plotting can be found in the Appendix (A4, A5, A6).

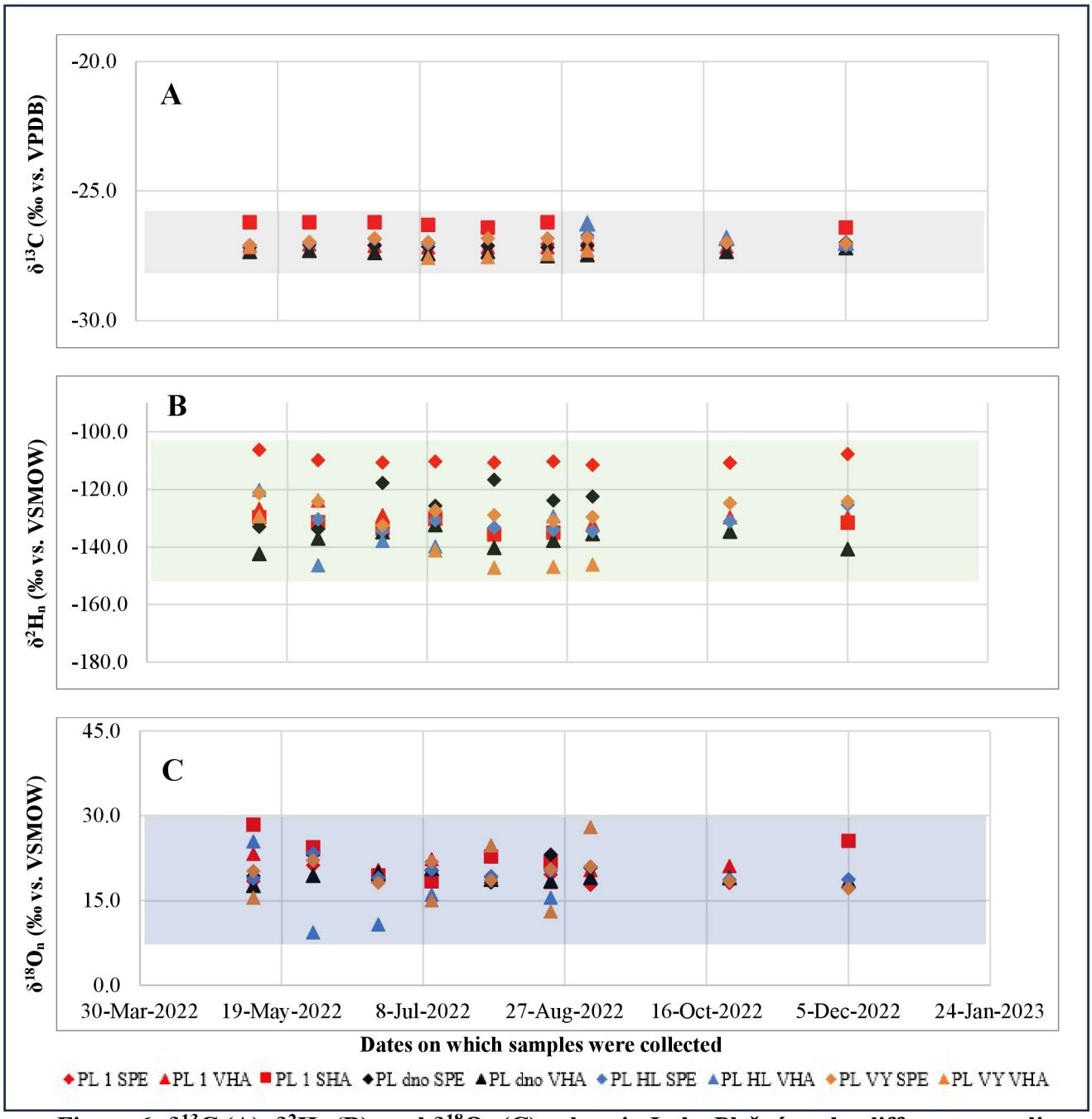

Figure 6: $\delta^{13}C$ (A), $\delta^{2}H_n$ (B), and $\delta^{18}O_n$ (C) values in Lake Plešné at the different sampling sites and DOM fractions. The boxes indicate the variability of the isotopic signal found for the three different stable isotopes. Outliers were identified and are not represented in the graph.

To compare the degree of variability in isotopic signals, the different isotopic composition ranges were compared to the typical observed standard error of $\delta^{13}C$, $\delta^{2}H_n$, and $\delta^{18}O_n$ measurements (0.2, 2.0, and 0.8 ‰, respectively). The $\delta^{13}C$ values exhibited relatively low variation, ranging from -26.2‰ to -27.6‰, with the typical error of the measurement being 0.2‰, the observed variation was ~7-fold greater. The $\delta^{2}H_n$ (B) values show a great variation with values ranging from -106‰

to -147‰, with the typical measurement error being 2.0‰ the value range corresponds to ~20 times the measurement error. The $\delta^{18}O_n$ (C) were plotted over a range of 9‰ to 29‰, corresponding to a range that was ~25-fold greater than the typical measurement error (0.8‰). The samples showed a wider variety of isotopic composition values during the spring and summer months, while tighter grouping was seen in the samples collected in late fall.

4.2.2 Hydrogen and Oxygen isotopes

The intrinsic hydrogen and oxygen isotopic compositions are plotted against each other in Figure 7. To be able to estimate isotopic fractionation of the water isotopes, the GMWL and the isotopic signatures of the water in addition to the sample fractions were plotted as well. The values used for plotting can be found in the Appendix (A4, A5, A6, A7).

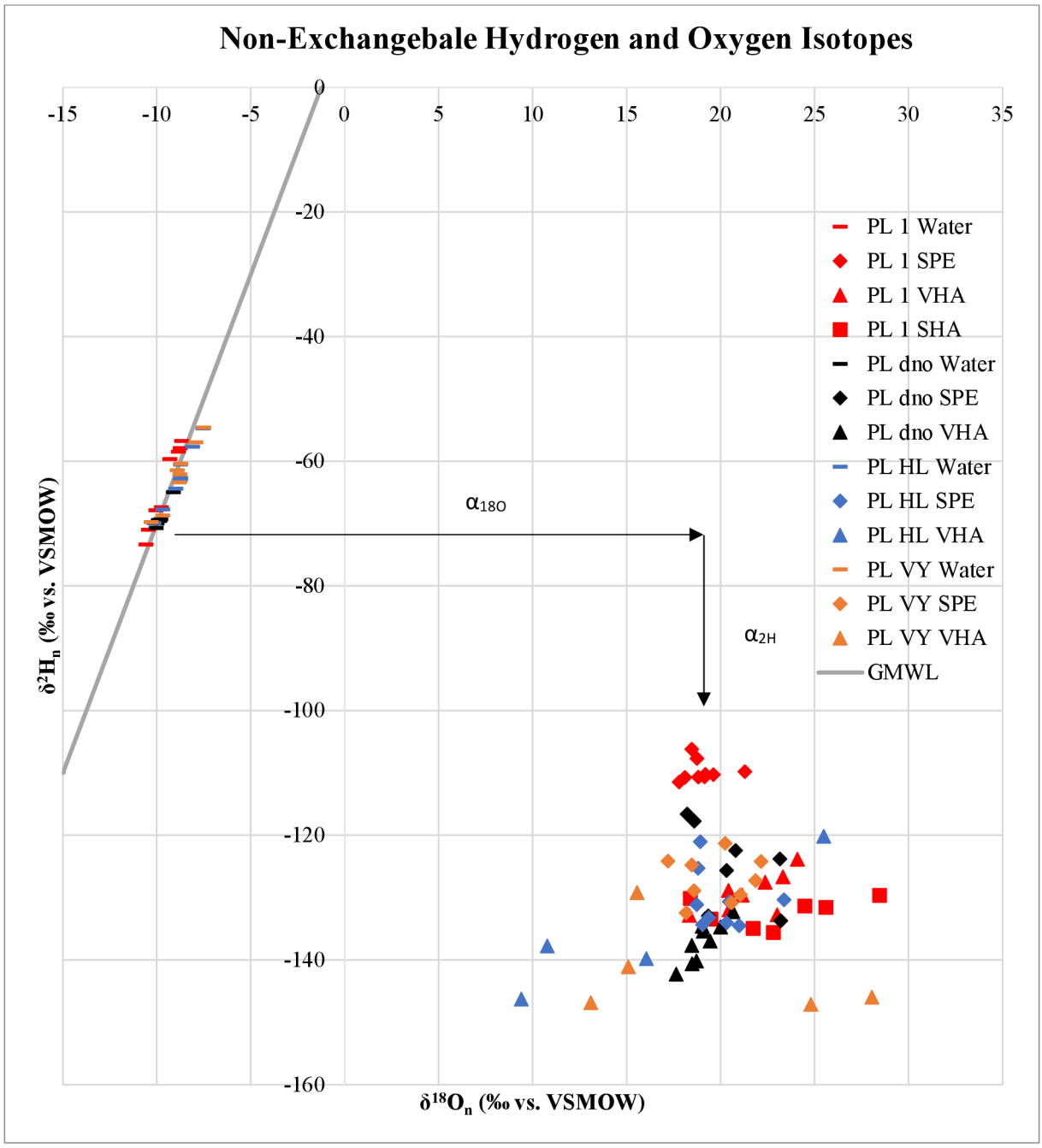

Figure 7: Non-exchangeable δ^2H_n and $\delta^{18}O_n$ in Lake Plešné for the different sampling sites and DOM fractions as well as the δ^2H and $\delta^{18}O$ values of the source water. The grey line depicts the GMWL and the arrows indicate the isotopic fractionation between the DOM and lake water. PL 1 is the inlet tributary, PL HL is surface water, PL dno is deep water, and PL VY is the exit tributary. Outliers were identified and are not represented in the graph.

The water isotopes measured for all 4 sampling sites show strong correlation with the global meteoric water line (GMWL), with no systematic trend between the different sampling sites observed. All water isotopes within the different DOM samples show an enrichment in ^{18}O and a

depletion in ^{2}H relative to lake water, whereby a narrower range for $\delta^{18}O_n$ values (+9‰ to +29‰) is observed compared to $\delta^{2}H_n$ values (-106‰ to -147‰). The SPE-DOM samples typically exhibited the highest $\delta^{2}H_n$ values and the narrowest range in $\delta^{18}O_n$ values. In contrast, the VHA and SHA samples are more scattered and show a broad range of measured $\delta^{18}O_n$ values and $\delta^{2}H_n$ values. PL HL and PL VY samples are the most depleted in ^{2}H and show great variability, particularly the VHA component isolated at these locations. Besides the SPE-DOM samples, tight grouping can only be seen for PL1 VHA and PL dno VHA samples.

To determine the variation of the DOM fractions compared to lake water the isotopic fractionation factors α_{2H} and α_{18O} were calculated according to Equation 6 and are summarized in Table 5. The whole table can be found in the Appendix (A4, A5, A6).

Table 5: Ranges of α_{2H} and α_{18O} values for all 4 sampling sites and 3 DOM fractions. The average was taken over a range of 8 samples (n=8) except for, PL1 SHA and PL dno SPE-DOM (n=6), PL VY VHA (n=4), and PL HL VHA (n=3).

	SPE-DOM		VHA		SHA	
	α_{18O}	α_{2H}	α_{18O}	α_{2H}	α_{18O}	α_{2H}
PL 1						
Range	1.027-1.032	0.943-0.965	1.029-1.035	0.931-0.943	1.027-1.039	0.916-0.939
Mean	1.029	0.951	1.032	0.931	1.033	0.929
PL dno						
Range	1.028-1.034	0.931-0.950	1.028-1.031	0.919-0.932	-	-
Mean	1.030	0.950	1.029	0.927	-	-
Pl HL						
Range	1.028-1.033	0.916-0.945	1.017-1.025	0.903-0.920	-	-
Mean	1.029	0.928	1.021	0.914	-	-
PL VY						
Range	1.026-1.032	0.921-0.945	1.024-1.036	0.903-0.936	-	-
Mean	1.029	0.931	1.030	0.914	-	-

To determine if there is a significant difference between the isotopic fractionation between the various groups and sampling sites, a paired t-test was conducted for all parameters mentioned above. To be able to compare the values in the most comprehensive way, only the sampling dates, where data for all groups was available, were compared.

No statistical significance was found between the isotopic fractionation factor of ^{18}O between any sampling site or DOM component, besides a statistical significant difference between the sampling sites PL HL and PL dno ($t(8)=2.584$, $p=0.04617$). Significant differences were found between the isotopic fraction factors of ^{2}H between all DOM components and sampling sites, with the exception of PL dno. For PL dno only PL HL showed a significantly different ^{2}H isotopic fractionation factor

(t(8)=2.584, p=0.03242), while the other sampling sites did not differ significantly in ^{2}H isotopic fraction factor from PL dno. The strongest differences in depletion and enrichment of deuterium relative to lake water were found between the SPE-DOM and VHA component (t(20)=12.026, p<.001) as well as between the SPE-DOM and SHA component (t(5)=-27.682, p<.001) where fractionation factors for VHA and SHA were typically stronger than for SPE-DOM, giving α_{2H} values further deviating from 1 (i.e., no isotopic fractionation). Additionally, the sampling site PL 1 showed strong deviations to the sampling sites PL HL (t(10)=10.262, p<.001) and PL VY (t(11)=10.658, p<.001). A table with all the statistical results can be found in the Appendix (A8).

4.3 Excitation Emission Matrix (EEM)

To elucidate the sources of the carbon found in different parts of the lake, excitation emission fluorescence spectra were determined. Three indices, namely the biological index, fluorescence index, and humification index are used for the investigation of the DOM pool. The indices are used to evaluate the recent autochthonous contribution, allochthonous contribution, and the extent of humification. The three indices are summarized in Table 6. All index values are reported in the Appendix (A9).

Table 6: Ranges of three different EEM indices values as well as their average value for the different sampling sites. The average was taken over a range of 6 values (n=6).

Sampling Site	Biological Index	Humification Index	Fluorescence Index
PL 1			
Range	0.607-0.642	0.833-0.884	1.147-1.194
Mean	0.619	0.849	1.172
PL VY			
Range	0.700-0.728	0.805-0.863	1.215-1.244
Mean	0.709	0.827	1.228
Pl dno			
Range	0.603-0.664	0.8113-0.863	1.187-1.248
Mean	0.643	0.824	1.221
PL HL			
Range	0.701-0.745	0.791-0.863	1.200-1.255
Mean	0.724	0.832	1.225

To determine if there was a significant difference of the origin of DOM found between the various sampling sites, an analysis of variance (ANOVA) was conducted for the three indices. A one-way ANOVA demonstrated that the location of sampling was significant for the recent autochthonous contribution (BIX), F(3,20)=36.27, p<.0.01, and allochthonous contribution compared to microbial contribution (FI), F(3,20)=11.61, p<0.01, to the DOM pool found at the sampling site. No

statistically significant relationship between the degree of humification (HIX) and sampling site was found, F(3,20)=1.499, p=.245.

To investigate seasonal variability in the contribution of different organic components to the DOM pool the three fluorescence indices were plotted in Figure 8. The values used for plotting can be found in the Appendix (A9).

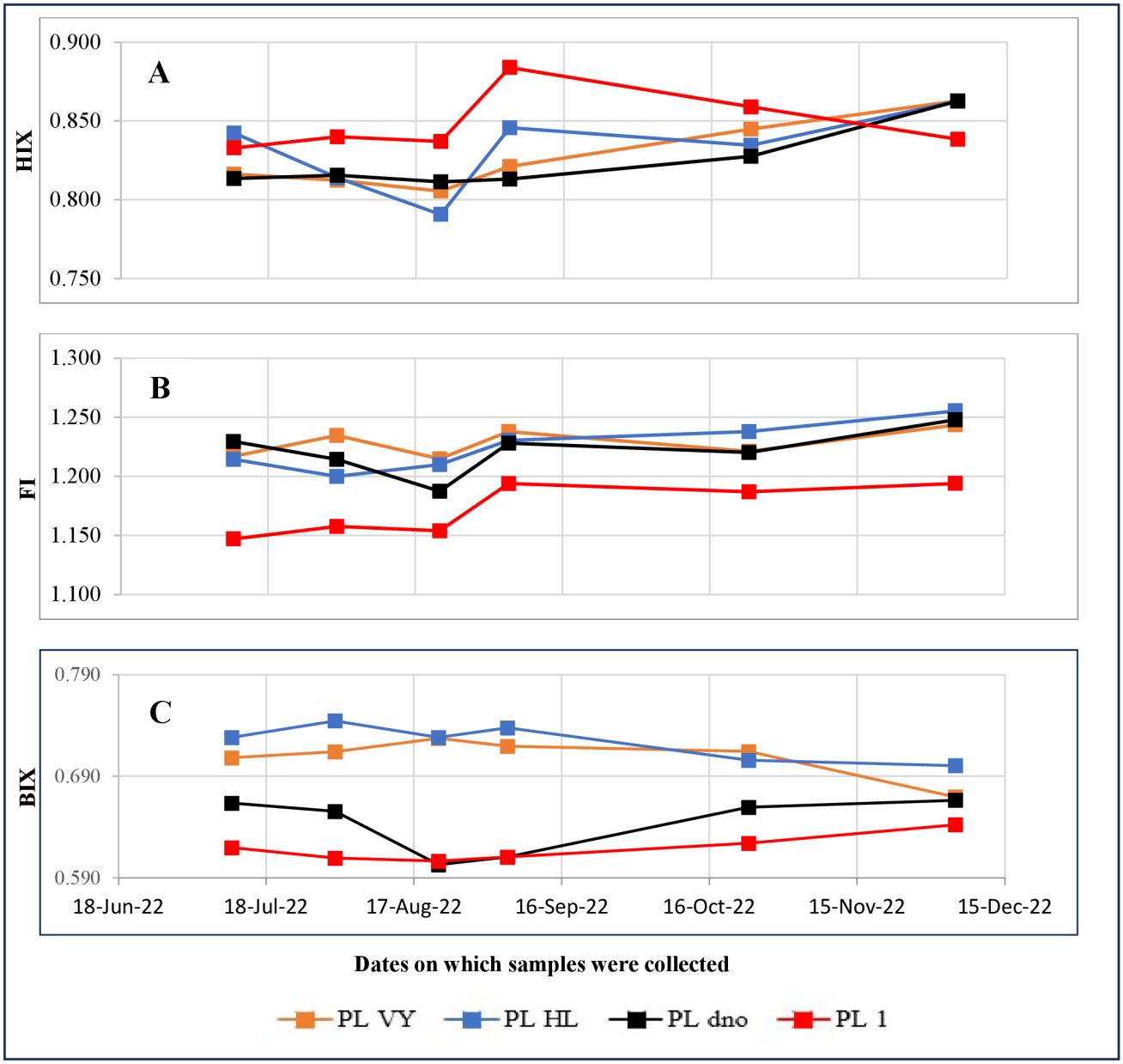

Figure 8: HIX (A), FI (B), and BIX (C) fluorescence indices collected from the different sampling sites.

The HIX (A) showed values ranging from 0.79 to 0.88 with the highest values found in the lake's inlet tributary. The lake's exit tributary, surface and deep water show similar values, where the

lowest values can be found in the summer months and the highest in fall and winter. The FI (B) showed values ranging from 1.15 to 1.26 with the highest signal found in the lake's exit tributary, surface and deep water in fall and winter. While these signals showed a similar trend and amplitude to each other, the lake's inlet tributary showed a unique signal that was always lower than the other sampling sites. The BIX (C) ranged from 0.61 to 0.75 with the highest signal measured in the lake's exit tributary and surface water. These two sampling sites showed a similar signal to each other, with the higher signal observed during summer and the lower values seen in fall and winter. The lowest signal belonged to the lake's exit tributary, with little variation observed during the sampling period. The lake's deep water exhibited values laying between the inlet and exit tributary.

4.4 Connection between stable hydrogen signatures and fluorescence indices

To investigate potential explanations of the high variability of the hydrogen isotopic signal (δ^2H_n), the δ^2H_n values were plotted against the fluorescence index and the biological index in Figures 9 and 10, respectively.

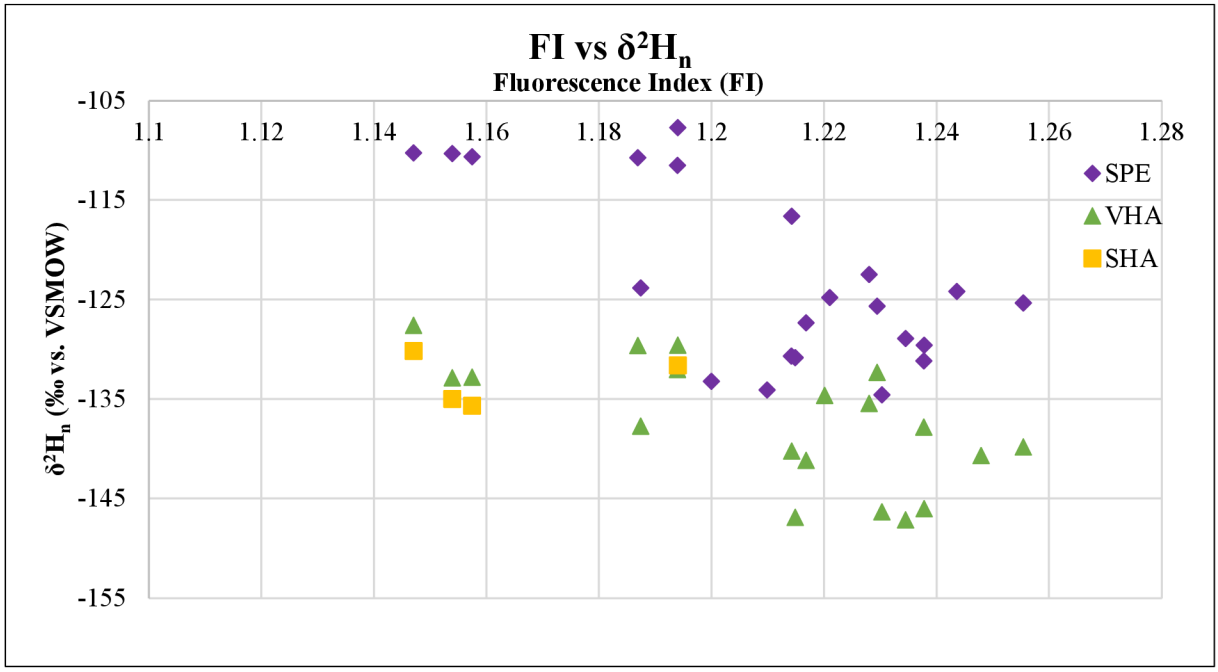

Figure 9: δ^2H_n values from the three DOM fractions plotted against the fluorescence index measured from the lake water.

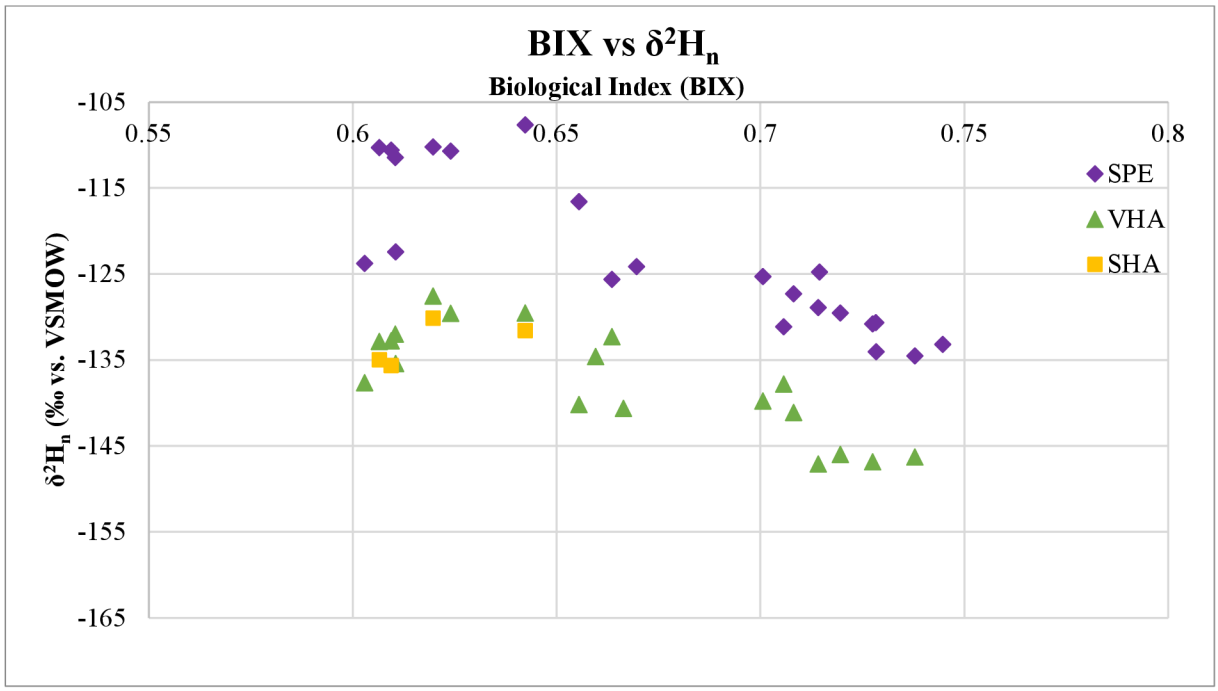

Figure 10: δ^2H_n values from the three DOM fractions plotted against the biological index measured from the lake water.

In Figure 9, a weak trend can be seen between the δ^2H_n values and the fluorescence index. Whereby, a greater depletion in ^2H can be observed with increasing FI index. The same trend was observed in Figure 10, whereby a greater depletion in ^2H can be observed with increasing BIX value. The SPE-DOM and VHA component followed this trend more closely than the trend observed in Figure 9. No distinguishable trend was observed between the δ^2H_n values and the humification index, the corresponding figure can be found in the Appendix (A10).

5. Discussion

5.1 DOC and DOM Extractions

A primary approach to assess seasonal variability in aquatic carbon fluxes is to investigate bulk DOC concentrations. The DOC concentrations in Plešné Lake (Figure 4) ranged from 10 mg L^{-1} to 24 mg L^{-1}, which shows a higher concentration and variability than the DOC concentrations measured in 2001 by Petr Porcal, where the concentrations ranged from 1.3 to 13.6 mg L^{-1} (Porcal et al., 2004). Little variations were observed between samples collected from the outlet tributary, deep and surface water. The inlet tributary, meanwhile, showed a higher DOC concentration than the other three sampling sites, likely owing to the low volume of the stream and contributions of soil porewater DOC.

The highest DOC concentrations at all sampling sites, excluding deep water, were typically observed in the summer months, July and August. The highest value was measured in the sample collected in July with the subsequent DOC measurements showing a decrease in DOC concentration. This trend is not only reflected in the DOC concentration, but also in the SPE-DOM concentration. This can be due to increase in precipitation, whereby the inlet tributary transports more DOM of terrestrial origin during the later summer months. This is due to more discharge of the inlet tributary, additionally due to more water, more organic matter is transported into the lake. This is reflected in the FI in the inlet tributary and surface water, where a higher contribution of terrestrial DOM to the DOM pool was observed in the summer samples, compared to the fall and winter samples (Figure 8). The higher temperatures and longer sunshine hours during the summer months, may then increase the activity of aqueous photosynthetic organisms, which would explain the increase in contribution of recent autochthonous DOM to the DOM pool. This trend is also reflected in the BIX of the lake's surface water and exit tributary (Figure 8). The deep water and inlet tributary seemed unaffected by the seasonal trends observed. This could be due to the colder water temperature and lower light intensity for the deeper parts of the lake. The constant flow of the inlet tributary may be a hindrance for the photosynthetic organisms thus, no such trend was observed. For an accurate interpretation of the seasonal signal observed, additional hydrometeorological data, especially precipitation, light intensity and discharge are needed. Furthermore, modelling hydrometeorological flow regimes would be outside the scope of this thesis.

The strong correlation between the outlet tributary and the lake's surface water, observed in all four figures (Figure 4, Figure 5, A2, A3), can be explained by the fact that the water discharged by the outlet tributary is the surface water of the lake.

For both the VHA and SHA fraction (A2 & A3) high values in the range of 150 to 170 mg L^{-1} were found. These high values are most likely not correct as the weight % of carbon for these samples were in the range of 0.8 to 6.9% (A5 & A6). In DOM isolated from inland waters, carbon usually comprises at least 20%, and typically ranges between 38.7 to 62.7% of the dry weight (Perdue & Richie, 2003). Another study reports similar values of 43.7 to 63.8% of carbon for humic acids from different sources (De Melo et al., 2016). The additional weight measured in VHA and SHA samples of the current study could arise from residual salt, which was not properly removed via the ion exchange resin. This indicates that the desalting procedure of SHA and VHA did not work as intended, which is supported by the observation for sampling site PL 1, for which it was calculated that more than 100% of the original DOC was extracted as the VHA and SHA fraction

(Table 4). As the PL 1 samples were processed after cleaning of the pump, organic residues leached from the pump could be the origin of the additional carbon in the sample. As the origin of the additional carbon cannot be identified, the results regarding PL 1 VHA and SHA fractions should be viewed with caution.

5.2 Stable C, H, and O isotope composition of Plešné Lake DOM

Stable carbon isotope ratio exhibited relatively little variability during the sampling period, with $\delta^{13}C$ values ranging from -26.2‰ to -27.6‰ and an average of -27.0‰. The observed $\delta^{13}C$ values are in accordance with the literature values for C_3 plants, which are -28.1‰ ± 2.5‰ (O'Leary, 1981). This is also reflected in the lake's surrounding vegetation, which is a regrowing conifer forest (Vystavna et al., 2021). Therefore, the DOM fractions are thought to originate from C_3 plants. Stable isotope ratios of hydrogen and oxygen showed a greater variability than those of carbon, with $\delta^{2}H_n$ and $\delta^{18}O_n$ values ranging from -106‰ to -147‰ and 9‰ to 29‰, respectively (Figure 6 & Figure 7). The SPE-DOM fraction showed the narrowest range of $\delta^{2}H_n$ and $\delta^{18}O_n$ values with -106‰ to -134‰ for the hydrogen isotopes and 17‰ to 23‰ for the oxygen isotopes. A similar range of the hydrogen and oxygen isotopic composition was found by Pilecky et al. in 2023, where a range of -115‰ to -140‰ and +9‰ to+15‰ was determined (Pilecky et al., 2023). The SHA and VHA components meanwhile show a greater variety of $\delta^{2}H_n$ and $\delta^{18}O_n$ values. This could be due to differences in origin or chemical transformations of the components making up the three DOM fractions.

To quantify the differences between the $\delta^{2}H_n$ and $\delta^{18}O_n$ values for the three DOM fractions, the isotopic fractionation factors α_{2H} and α_{180} were determined and compared via a paired t-test. The α_{18O} isotopic fractionation factor indicated an enrichment in ^{18}O compared to lake water, with mean values of the SPE-DOM, VHA, and SHA of ranging from 1.029 to 1.030, 1.021 to 1.032, and 1.033, respectively (Table 5). No statistically significant difference was found for the relative enrichment in ^{18}O between any of the three samples and four sampling sites, with the exception of PL HL and PL dno. A similar α_{18O} isotopic fractionation factor of 1.027±0.02 was determined for freshwater vascular plants by DeNiro & Epstein in 1981, who attributed the enrichment in ^{18}O in cellulose compared to its source water to the stronger bonding of the heavier O isotope in the carbonyl bond (DeNiro & Epstein in 1981). The high similarity in $\alpha_{18O,}$ suggests that the origin of many molecules comprising the SPE-DOM, VHA, and SHA fraction could be cellulose or organic matter which was produced via a similar biosynthetic mechanism, and therefore maintains a similar

enrichment in ^{18}O relative to source water. These molecules could then undergo further transformations along the aquatic continuum and thereby exhibit the range of values observed.

A strong statistical difference was found between the α_{2H} values of the fractions SPE-DOM and SHA, SPE-DOM and VHA, and the sampling sites PL 1 and PL VY and PL1 and PL HL. In particular, SHA and VHA samples showed a significantly greater depletion in ^{2}H compared to SPE-DOM, and the DOM extracted from the inlet tributary (PL 1) showed a significantly greater enrichment compared to the outlet tributary (PL VY) and surface water (PL HL). This trend could arise from chemical differences among the DOM components, with the SHA and VHA fractions both comprising organic acids, albeit with differing polarity, while SPE-DOM typically comprises more hydrophobic molecules that attach to the polystyrene-divinyl-benzene solid phase of the PPL cartridge. The DOM extracted from the lake's inlet tributary showed greatly differing α_{2H} values compared to the lake's surface water and outlet tributary. The differences could be caused due to differences in the source of the DOM, which was also suggested by the BIX and FI indices. That is, the DOM pool of the lake's inlet tributary is characterised by a smaller contribution of recently produced organic matter and microbial fulvic acids, compared to the lake's exit tributary and surface water (Figure 8 & Table 6). The statistical results should be interpreted with care as many results show a low degree of freedom, as many measurements had to be neglected due to the low C%.

5.3 Excitation Emission Matrix

The EEM was used to investigate the chromophoric properties of DOM in a water sample and three indices, namely the humification index, the biological index, and the fluorescence index, were derived from it. The three indices were used to distinguish the contribution of different sources to the whole DOM pool. Additionally, the influence of the sampling site on the three indices was investigated via an analysis of variance.

A one-way ANOVA demonstrated that the location of sampling was statistically significant for the recent autochthonous contribution (BIX) and allochthonous contribution, compared to microbial contribution, (FI) to the DOM pool at the sampling site. The indices ranged from 0.619 to 0.724 and 1.172 to 1.228, respectively (Table 6). The values obtained for the FI are similar to values found in the literature, which range from 1.2 to 1.8 for natural waters. Low FI values indicate a terrestrial origin of DOM, while high values indicate a microbial origin of DOM (Hansen et al., 2016). The DOM found in the inlet tributary showed a significantly higher fraction of terrestrial sources to the DOM pool, than the other sampling sites. The other sampling sites showed, even

though not to the extent of the inlet tributary, also a high contribution of terrestrial sources to the DOM pool and therefore only a low contribution of microbial sources (Hansen et al., 2016; McKnight et al., 2001).

The values obtained for the BIX are similar to values found in the literature, which range from 0.53 to 0.92 for a watershed located in South Bohemia (Vogt et al., 2023). High BIX values, >1, indicate recently produced, autochthonous DOM (Hansen et al., 2016). The DOM pool located at the lake surface water and outlet tributary shows a significantly higher recent autochthonous contribution to the DOM pool than the inlet tributary and the lake deep water. The degree of humification of the DOM pool showed no statistically significant differences between sampling sites, with values ranging from 0.824 to 0.849 (Table 6 & Figure 8). The HIX values observed are in accordance with values reported in other studies, which often range between 0.6 and 0.9 (Hansen et al., 2016).

The DOM pool of the surface water showed a significantly higher contribution of recently photosynthesised material, this could be due greater exposure to sunlight than the deeper parts of the lake, while also experiencing less turbulence than the inlet tributary. This idea is further supported by the higher contribution of recently photosynthesized materials during the summer months and early fall (Figure 8). The inlet tributary showed a significantly higher contribution of terrestrial DOM to the DOM pool, this could be due to constant water movement along the river, whereby more organic material of terrestrial origin can be incorporated and transported. The high coupling observed between the outlet tributary and surface water can once again be explained by the fact that the water discharged by the outlet tributary is the surface water of the lake.

5.4 Connection between stable hydrogen signatures and fluorescence indices

Hydrogen exhibited the greatest range of values of any stable isotopic signature investigated (Figure 6). Therefore, the δ^2H_n values show the greatest potential in differing between sampling sites and DOM fractions and may further be applicable to identify DOM fluxes. To investigate this diverse isotope and explain some of the variability observed, the δ^2H_n values were plotted against the fluorescence index and biological index in Figures 9 and 10, respectively. A weak trend, namely depletion of ^2H with increasing contribution of microbial fulvic acids (i.e., lower FI values) to DOM was observed (Figure 9). This suggests that fulvic acids of microbial origin may have characteristically low δ^2H_n values. These differences may occur due to isotopic fractionation occurring during microbial metabolism and should be assessed in future experiments.

Similarly, increasing contributions of recent autochthonous organic matter to the DOM pool corresponded to increasing depletion of ^{2}H. One interpretation of this finding is that the autochthonous organic matter is more depleted in ^{2}H compared to the organic matter derived from other sources. This could be due to differing isotopic fractionation for photosynthesis taking place in an aqueous environment, compared to a terrestrial environment. The differences occurring may be due to differing temperature, access to water, and light intensity, among other factors.

6. Conclusions

This thesis reports among the first stable hydrogen and oxygen isotope ratio data for DOM isolated from natural waters. Notably, the variability observed in $\delta^{2}H_{n}$ and $\delta^{18}O_{n}$ values was greater than that observed for $\delta^{13}C$, also when normalized by the error of the respective isotope measurements. This finding supports further development of these novel proxies as tracers of DOM fluxes in the environment. These parameters were measured for DOM isolated using classical extraction protocols, for which trends in $\delta^{2}H_{n}$ and $\delta^{18}O_{n}$ values could be observed between sites and other environmental indices. The SPE-DOM fraction did not only exhibit the most robust trends (Figure 9 & Figure 10), but it also exhibited the most stability in terms of isotopic composition, which likely stems from the reliability and reproducibility of the extraction method. The extraction method used to isolate VHA and SHA showed a greater variability in concentration, isotopic signal, and correlation with fluorescent indices. The SHA fraction in particular showed a wider range of values than the VHA fraction. This finding is consistent with the greater number of outliers found in this fraction (A6). It is thought that the scattered and faulty values are caused by problems in the pH neutralisation protocol, especially for the SHA fraction. This conclusion is supported by the lower %C found in the SHA fraction compared to the VHA and SPE-DOM fraction. In conclusion, the SPE-DOM component described in this thesis likely exhibited the strongest trends because this material was more amenable to subsequent analyses than the saltier DOM isolated from DAX and XAD resins.

Although this thesis shows that trends between the $\delta^{2}H_{n}$ and fluorescent indices exist, these trends are only followed weakly by the different DOM fractions and need to be explored further. Therefore, the most important contribution of this thesis may be that the variability of $\delta^{2}H_{n}$ and $\delta^{18}O_{n}$ in DOM observed in the natural setting in Plešné Lake may inspire intriguing questions for future studies.

References

Bauer, J. E., Cai, W. J., Raymond, P. A., Bianchi, T. S., Hopkinson, C. S., & Regnier, P. A. (2013). The changing carbon cycle of the coastal ocean. Nature, 504(7478), 61-70. https://doi.org/10.1038/nature12857

Bouwman, A. F., Bierkens, M. F. P., Griffioen, J., Hefting, M. M., Middelburg, J. J., Middelkoop, H., & Slomp, C. P. (2013). Nutrient dynamics, transfer and retention along the aquatic continuum from land to ocean: towards integration of ecological and biogeochemical models. Biogeosciences, 10(1), 1-22. https://doi.org/10.5194/bg-10-1-2013

Bushaw, K. L., Zepp, R. G., Tarr, M. A., Schulz-Jander, D., Bourbonniere, R. A., Hodson, R. E., ... & Moran, M. A. (1996). Photochemical release of biologically available nitrogen from aquatic dissolved organic matter. Nature, 381(6581), 404-407. https://doi.org/10.1038/381404a0

Chow, C. W., Fabris, R., & Drikas, M. (2004). A rapid fractionation technique to characterise natural organic matter for the optimisation of water treatment processes. Journal of Water Supply: Research and Technology—Aqua, 53(2), 85-92. https://doi.org/10.2166/aqua.2004.0008

Coplen, T. B., Böhlke, J. K., De Bievre, P., Ding, T., Holden, N. E., Hopple, J. A., ... & Xiao, Y. (2002). Isotope-abundance variations of selected elements (IUPAC Technical Report). Pure and applied chemistry, 74(10), 1987-2017. https://doi.org/10.1351/pac200274101987

Craig, H. (1961). Isotopic variations in meteoric waters. Science, 133(3465), 1702-1703. DOI: 10.1126/science.133.3465.1702

Crum, R. H., Murphy, E. M., & Keller, C. K. (1996). A non-adsorptive method for the isolation and fractionation of natural dissolved organic carbon. Water Research, 30(5), 1304-1311. https://doi.org/10.1016/0043-1354(95)00279-0

DeMelo, B. A. G., Motta, F. L., & Santana, M. H. A. (2016). Humic acids: Structural properties and multiple functionalities for novel technological developments. Materials Science and Engineering: C, 62, 967-974. https://doi.org/10.1016/j.msec.2015.12.001

DeNiro, M. J., & Epstein, S. (1981). Isotopic composition of cellulose from aquatic organisms. Geochimica et Cosmochimica Acta, 45(10), 1885-1894. https://doi.org/10.1016/0016-7037(81)90018-1

Dittmar, T., Koch, B., Hertkorn, N., & Kattner, G. (2008). A simple and efficient method for the solid-phase extraction of dissolved organic matter (SPE-DOM) from seawater. Limnology and Oceanography: Methods, 6(6), 230-235. https://doi.org/10.4319/lom.2008.6.230

Drake, T. W., Raymond, P. A., & Spencer, R. G. (2018). Terrestrial carbon inputs to inland waters: A current synthesis of estimates and uncertainty. Limnology and Oceanography Letters, 3(3), 132-142. https://doi.org/10.1002/lol2.10055

Ehleringer, J. R., Cerling, T. E., West, J. B., Podlesak, D. W., Chesson, L. A., & Bowen, G. J. (2008). Spatial considerations of stable isotope analyses in environmental forensics. https://doi.org/10.1039/9781847558343-00036

Flores, R. M. (2014). Chapter 3-Origin of Coal as Gas Source and Reservoir Rocks. Coal and Coalbed Gas, 97-165. https://doi.org/10.1016/B978-0-12-396972-9.00003-3

Francko, D. A., & Heath, R. T. (1982). UV-sensitive complex phosphorus: Association with dissolved humic material and iron in a bog lake 1. Limnology and Oceanography, 27(3), 564-569. https://doi.org/10.4319/lo.1982.27.3.0564

Hansen, A. M., Kraus, T. E., Pellerin, B. A., Fleck, J. A., Downing, B. D., & Bergamaschi, B. A. (2016). Optical properties of dissolved organic matter (DOM): Effects of biological and photolytic degradation. Limnology and oceanography, 61(3), 1015-1032. https://doi.org/10.1002/lno.10270

Hoefs, J. (2015). Stable isotope geochemistry. 7th Edition. Berlin: springer. https://doi.org/10.1007/978-3-319-19716-6

Hudson, N., Baker, A., & Reynolds, D. (2007). Fluorescence analysis of dissolved organic matter in natural, waste and polluted waters—a review. River research and applications, 23(6), 631-649. https://doi.org/10.1002/rra.1005

Kendall, C., & Caldwell, E. A. (1998). Fundamentals of isotope geochemistry. In Isotope tracers in catchment hydrology (pp. 51-86). Elsevier. https://doi.org/10.1016/B978-0-444-81546-0.50009-4

Leenheer, J. A. (1981). Comprehensive approach to preparative isolation and fractionation of dissolved organic carbon from natural waters and wastewaters. Environmental science & technology, 15(5), 578-587.

Leenheer, J. A., & Croué, J. P. (2003). Peer reviewed: characterizing aquatic dissolved organic matter. Environmental science & technology, 37(1), 18A-26A.

Ludwig, W., Probst, J. L., & Kempe, S. (1996). Predicting the oceanic input of organic carbon by continental erosion. Global Biogeochemical Cycles, 10(1), 23-41. https://doi.org/10.1029/95GB02925

Malhi, Y. (2002). Carbon in the atmosphere and terrestrial biosphere in the 21st century. Philosophical Transactions of the Royal Society of London. Series A: Mathematical, Physical and Engineering Sciences, 360(1801), 2925-2945. https://doi.org/10.1098/rsta.2002.1098

McKnight, D. M., Boyer, E. W., Westerhoff, P. K., Doran, P. T., Kulbe, T., & Andersen, D. T. (2001). Spectrofluorometric characterization of dissolved organic matter for indication of precursor organic material and aromaticity. Limnology and Oceanography, 46(1), 38-48. https://doi.org/10.4319/lo.2001.46.1.0038

Meador, T. B., & Aluwihare, L. I. (2014). Production of dissolved organic carbon enriched in deoxy sugars representing an additional sink for biological C drawdown in the Amazon River plume. Global Biogeochemical Cycles, 28(10), 1149-1161. https://doi.org/10.1002/2013GB004778

O'Leary, M. H. (1981). Carbon isotope fractionation in plants. Phytochemistry, 20(4), 553-567. https://doi.org/10.1016/0031-9422(81)85134-5

Perdue, E. M., & Ritchie, J. D. (2003). Dissolved organic matter in freshwaters. Treatise on geochemistry, 5, 605. https://doi.org/10.1016/B0-08-043751-6/05080-5

Pilecky, M., Meador, T. B., Kämmer, S. K., Winter, K., Ptacnikova, R., Wassenaar, L. I., & Kainz, M. J. (2023). Response of stable isotopes (δ2H, δ13C, δ15N, δ18O) of lake water, dissolved organic matter, seston, and zooplankton to an extreme precipitation event. Science of The Total Environment, 891, 164622. https://doi.org/10.1016/j.scitotenv.2023.164622

Porcal, P., Hejzlar, J., & Kopáček, J. (2004). Seasonal and photochemical changes of DOM in an acidified forest lake and its tributaries. Aquatic sciences, 66, 211-222. https://doi.org/10.1007/s00027-004-0701-1

Raymond, P. A., & Spencer, R. G. (2015). riverine DOM. In Biogeochemistry of marine dissolved organic matter (pp. 509-533). Academic Press. https://doi.org/10.1016/B978-0-12-405940-5.00011-X

Regnier, P., Friedlingstein, P., Ciais, P., Mackenzie, F. T., Gruber, N., Janssens, I. A., Laruelle, G. G., Lauerwald, R., Luyssaert, S., Andersson, A. J., Arndt, S., Arnosti, C., Borges, A. V., Dale, A. W., Gallego-Sala, A., Goddéris, Y., Goossens, N., Hartmann, J., Heinze, C., . . . &

Thullner, M. (2013). Anthropogenic perturbation of the carbon fluxes from land to ocean. Nature Geoscience, 6(8), 597–607. https://doi.org/10.1038/ngeo1830

Rosman, K. J. R., & Taylor, P. D. P. (1999). Table of isotopic masses and natural abundances. Pure and Applied Chemistry, 71, 1593-1607.

Salonen, K., & Hammar, T. (1986). On the importance of dissolved organic matter in the nutrition of zooplankton in some lake waters. Oecologia, 68, 246-253. https://doi.org/10.1007/BF00384795

Sarmiento, J. L., & Sundquist, E. T. (1992). Revised budget for the oceanic uptake of anthropogenic carbon dioxide. Nature, 356(6370), 589-593. https://doi.org/10.1038/356589a0

Shapiro, J. (1957). Chemical and Biological Studies on the Yellow Organic Acids of Lake Water 1. Limnology and Oceanography, 2(3), 161-179. https://doi.org/10.1002/lno.1957.2.3.0161

Sharp, Z. (2017). Principles of stable isotope geochemistry. https://doi.org/10.25844/h9q1-0p82

Stets, E. G., Striegl, R. G., Aiken, G. R., Rosenberry, D. O., & Winter, T. C. (2009). Hydrologic support of carbon dioxide flux revealed by whole-lake carbon budgets. Journal of geophysical research: Biogeosciences, 114(G1). https://doi.org/10.1029/2008JG000783

Tranvik, L. J. (1992). Allochthonous dissolved organic matter as an energy source for pelagic bacteria and the concept of the microbial loop. Dissolved organic matter in lacustrine ecosystems: Energy source and system regulator, 107-114. https://doi.org/10.1007/978-94-011-2474-4_8

Ussiri, D.A., Lal, R. (2017). Introduction to Global Carbon Cycling: An Overview of the Global Carbon Cycle. In: Carbon Sequestration for Climate Change Mitigation and Adaptation. Springer, Cham. https://doi.org/10.1007/978-3-319-53845-7_3

van Heemst, J. D., Megens, L., Hatcher, P. G., & de Leeuw, J. W. (2000). Nature, origin and average age of estuarine ultrafiltered dissolved organic matter as determined by molecular and carbon isotope characterization. Organic geochemistry, 31(9), 847-857. https://doi.org/10.1016/S0146-6380(00)00059-0

Vogt, R. D., Porcal, P., Hejzlar, J., Paule-Mercado, M. C., Haaland, S., Gundersen, C. B., Orderud, G. I., & Eikebrokk, B. (2023). Distinguishing between Sources of Natural Dissolved Organic Matter (DOM) Based on Its Characteristics. Water, 15(16), 3006. https://doi.org/10.3390/w15163006

Vystavna, Y., Paule-Mercado, M., Juras, R., Schmidt, S. I., Kopáček, J., Hejzlar, J., & Huneau, F. (2021). Effect of snowmelt on the dynamics, isotopic and chemical composition of runoff in mature and regenerated forested catchments. Journal of Hydrology, 598, 126437. https://doi.org/10.1016/j.jhydrol.2021.126437

Wassenaar, L. I., Sisti, L., Pilecky, M., & Kainz, M. (2023). Reproducible measurements of the δ2H composition of non-exchangeable hydrogen in complex organic materials using the UniPrep2 online static vapour equilibration and sample drying system. MethodsX, 10, 101984. https://doi.org/10.1016/j.mex.2022.101984

Xu, X., Kang, J., Shen, J., Zhao, S., Wang, B., Zhang, X., & Chen, Z. (2021). EEM–PARAFAC characterization of dissolved organic matter and its relationship with disinfection by-products formation potential in drinking water sources of northeastern China. *Science of the Total Environment*, *774*, 145297. https://doi.org/10.1016/j.scitotenv.2021.145297

Ye, F., Guo, W., Wei, G., & Jia, G. (2018). The sources and transformations of dissolved organic matter in the Pearl River Estuary, China, as revealed by stable isotopes. Journal of Geophysical Research: Oceans, 123(9), 6893-6908. https://doi.org/10.1029/2018JC014004

Zhang, Y., Gan, Y., Yu, K., & Han, L. (2021). Fractionation of carbon isotopes of dissolved organic matter adsorbed to goethite in the presence of arsenic to study the origin of DOM in groundwater. Environmental Geochemistry and Health, 43, 1225-1238. https://doi.org/10.1007/s10653-020-00644-w

Appendix

A 1: DOM concentrations of the four sampling sites. Samples were collected over a time frame of half a year.

Sampling Site	C_{VHA} / mg L^{-1}	C_{SHA} / mg L^{-1}	C_{SPE} / mg L^{-1}
PL 1 09.05.2022	29.9	6.2	24.8
PL 1 30.05.2022	26.5	6.8	16.2
PL 1 22.06.2022	26.8	7.9	19.1
PL 1 11.07.2022	35.9	11.8	25.5
PL 1 01.08.2022	34.7	13.3	22.5
PL 1 22.08.2022	31.8	8.1	16
PL 1 05.09.2022	29.5	-	18.7
PL 1 24.10.2022	36.7	14.9	26.4
PL 1 05.12.2022	29.6	4.0	21
PL dno 09.05.2022	16.3	7.2	11
PL dno 30.05.2022	15.3	3.9	14.8
PL dno 22.06.2022	14.1	8.3	9.4
PL dno 11.07.2022	17.6	4.5	8.5
PL dno 01.08.2022	18.2	6.1	9.2
PL dno 22.08.2022	15.4	4.6	8.2
PL dno 05.09.2022	12.9	4.8	11.1
PL dno 24.10.2022	12.0	5.2	11.6
PL dno 05.12.2022	16.3	6.4	8.1
PL HL 09.05.2022	148.8	166.3	11.2
PL HL 30.05.2022	24.6	7.7	15.8
PL HL 22.06.2022	163.8	26.3	9.1
PL HL 11.07.2022	126.7	64.1	13.5
PL HL 01.08.2022	131.4	11.4	10.5
PL HL 22.08.2022	41.8	2.2	8.2
PL HL 05.09.2022	22.5	2.6	6.3
PL HL 24.10.2022	19.7	4.2	13.1
PL HL 05.12.2022	25.1	7.1	6.7
PL VY 09.05.2022	9.4	0.6	11.4
PL VY 30.05.2022	11.2	6.2	15.3
PL VY 22.06.2022	107.3	114.0	9.3
PL VY 11.07.2022	18.0	4.9	16.9
PL VY 01.08.2022	19.4	5.8	10
PL VY 22.08.2022	19.3	2.9	7.7
PL VY 05.09.2022	19.8	5.8	7.2
PL VY 24.10.2022	24.3	7.2	11.8
PL VY 05.12.2022	30.1	8.0	7.6

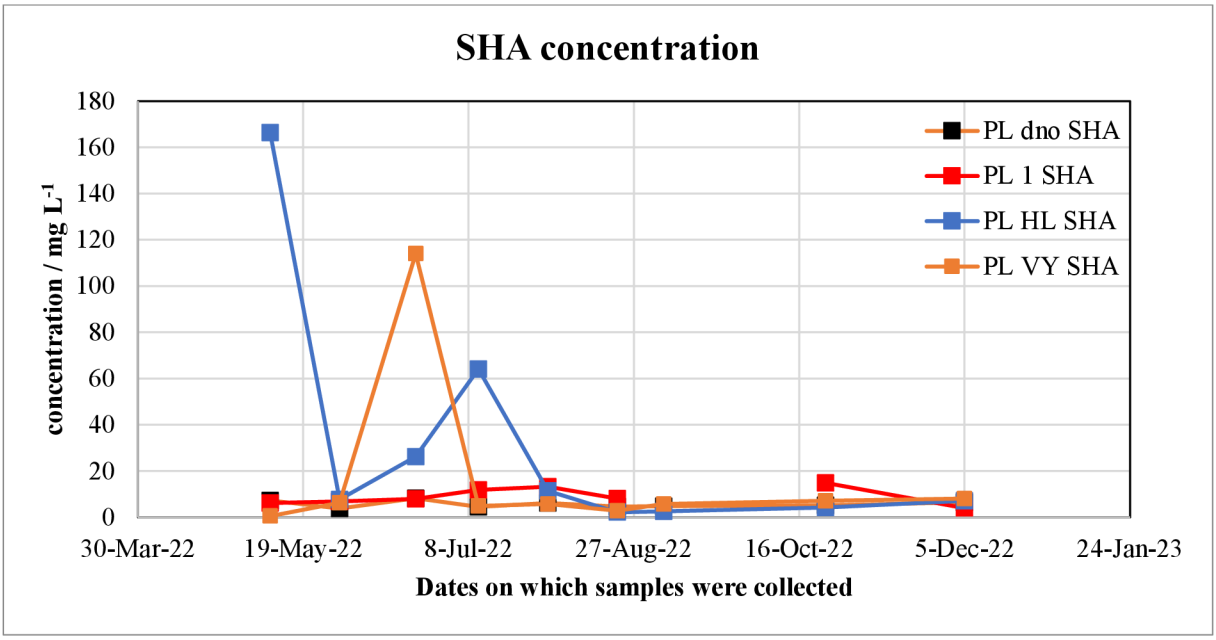

A2: SHA concentration in Lake Plešné. PL 1 is the inlet tributary, PL HL is surface water, PL dno is deep water, and PL VY is the exit tributary. The PL 1 sample from 05.09.2022 is missing.

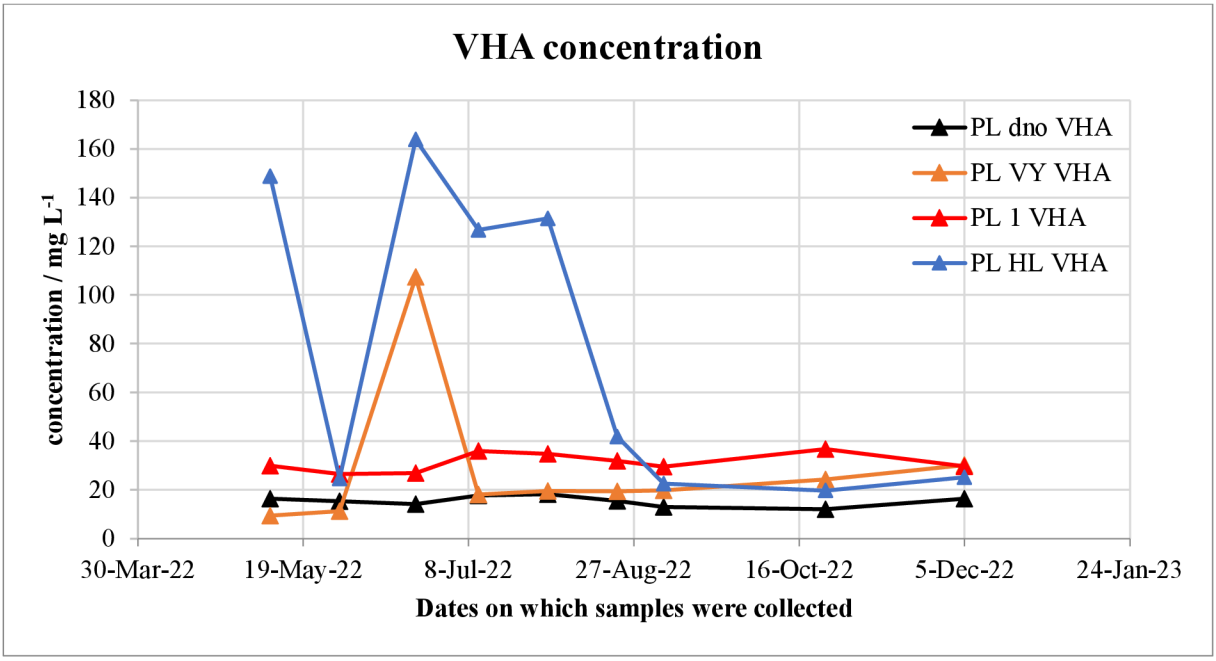

A3: VHA concentration in Lake Plešné. PL 1 is the inlet tributary, PL HL is surface water, PL dno is deep water, and PL VY is the exit tributary.

A4: Stable isotopic signal ($\delta^{13}C$, $\delta^{2}H_n$, $\delta^{18}O_n$), the isotopic fractionation factors (α_{2H}, α_{18O}) and the weight percentage of carbon of the SPE-DOM component.

Sampling Site	% C	$\delta^{13}C$	$\delta^{2}H_n$	α_{2H}	$\delta^{18}O_n$	α_{18O}
PL 1 09.05.2022	37.7%	-27.1	-106.2	0.965	18.5	1.029
PL 1 30.05.2022	36.8%	-27.0	-109.8	0.958	21.3	1.032

PL 1 22.06.2022	40.3%	-27.1	-110.7	0.954	18.8	1.029
PL 1 11.07.2022	33.4%	-27.0	-110.2	0.945	19.2	1.028
PL 1 01.08.2022	42.4%	-27.1	-110.6	0.943	19.2	1.028
PL 1 22.08.2022	40.7%	-27.1	-110.3	-	19.6	-
PL 1 05.09.2022	44.4%	-27.0	-111.5	0.943	17.8	1.027
PL 1 24.10.2022	48.7%	-27.0	-110.7	0.946	18.1	1.028
PL 1 05.12.2022	41.4%	-27.1	-107.7	0.957	18.7	1.029
PL dno 09.05.2022	35.1%	-27.2	-132.9	0.932	19.4	1.029
PL dno 30.05.2022	45.9%	-27.1	-133.7	0.931	23.2	1.034
PL dno 22.06.2022	40.9%	-27.1	-117.7	0.948	18.6	1.029
PL dno 11.07.2022	47.8%	-27.1	-125.6	0.940	20.3	1.031
PL dno 01.08.2022	38.6%	-27.1	-116.6	0.950	18.2	1.028
PL dno 22.08.2022	59.6%	-27.2	-123.8	-	23.2	-
PL dno 05.09.2022	46.2%	-27.1	-122.4	0.944	20.8	1.031
PL dno 24.10.2022	46.8%	-27.0	-	-	-	-
PL dno 05.12.2022	50.9%	-27.0	-	-	-	-
PL HL 09.05.2022	59.1%	-27.1	-121.1	0.945	18.9	1.029
PL HL 30.05.2022	48.1%	-27.0	-130.4	0.933	23.4	1.033
PL HL 22.06.2022	34.5%	-26.8	-134.3	0.924	19.0	1.028
PL HL 11.07.2022	39.7%	-27.0	-130.7	0.925	20.5	1.029
PL HL 01.08.2022	43.3%	-26.8	-133.2	0.920	19.4	1.028
PL HL 22.08.2022	43.5%	-26.8	-134.0	0.916	20.3	1.028
PL HL 05.09.2022	47.1%	-26.7	-134.5	-	21.0	-
PL HL 24.10.2022	26.0%	-27.0	-131.1	0.927	18.7	1.028
PL HL 05.12.2022	44.7%	-27.1	-125.3	0.935	18.8	1.028
PL VY 09.05.2022	47.0%	-27.1	-121.3	0.945	20.3	1.031
PL VY 30.05.2022	36.9%	-27.0	-124.2	0.940	22.2	1.032
PL VY 22.06.2022	31.7%	-26.8	-132.5	0.926	18.2	1.027
PL VY 11.07.2022	30.7%	-27.0	-127.3	0.929	21.9	1.031
PL VY 01.08.2022	47.4%	-26.8	-128.9	0.924	18.6	1.027
PL VY 22.08.2022	74.8%	-26.8	-130.8	0.919	20.6	1.028
PL VY 05.09.2022	48.7%	-26.8	-129.5	-	21.1	-
PL VY 24.10.2022	48.7%	-27.0	-124.8	0.933	18.5	1.027
PL VY 05.12.2022	49.7%	-27.0	-124.1	0.933	17.2	1.026

A5: Stable isotopic signal ($\delta^{13}C$, $\delta^{2}H_n$, $\delta^{18}O_n$), the isotopic fractionation factors (α_{2H}, α_{18O}) and the weight percentage of carbon of the VHA component.

Sampling Site	% C	$\delta^{13}C$	$\delta^{2}H_n$	α_{2H}	$\delta^{18}O_n$	α_{18O}
PL 1 09.05.2022	38.7%	-27.1	-126.7	0.942	23.3	1.034
PL 1 30.05.2022	42.8%	-27.0	-123.8	0.943	24.1	1.035
PL 1 22.06.2022	42.0%	-27.1	-128.9	0.934	20.4	1.030
PL 1 11.07.2022	37.8%	-27.2	-127.6	0.927	22.4	1.032
PL 1 01.08.2022	34.6%	-27.2	-132.8	0.919	23.0	1.032
PL 1 22.08.2022	29.7%	-27.2	-132.8	-	18.3	-
PL 1 05.09.2022	35.5%	-27.1	-132.0	0.921	20.5	1.029
PL 1 24.10.2022	32.4%	-27.1	-129.6	0.926	21.2	1.031
PL 1 05.12.2022	37.9%	-26.9	-129.5	0.934	18.5	1.029

PL dno 09.05.2022	28.1%	-27.3	-142.3	0.922	17.6	1.028
PL dno 30.05.2022	27.4%	-27.3	-137.0	0.928	19.4	1.030
PL dno 22.06.2022	28.0%	-27.4	-134.7	0.930	20.0	1.030
PL dno 11.07.2022	25.7%	-27.4	-132.3	0.932	20.7	1.031
PL dno 01.08.2022	26.9%	-27.3	-140.2	0.924	18.7	1.029
PL dno 22.08.2022	24.1%	-27.5	-137.7	-	18.5	-
PL dno 05.09.2022	26.9%	-27.5	-135.4	0.930	19.1	1.029
PL dno 24.10.2022	30.1%	-27.3	-134.6	0.931	19.0	1.029
PL dno 05.12.2022	30.2%	-27.2	-140.6	0.919	18.5	1.028
PL HL 09.05.2022			-120.1	0.946	25.5	1.036
PL HL 30.05.2022	17.5%	-26.5	-150.2	0.912	15.1	1.025
PL HL 22.06.2022	14.6%	-19.5	-127.3	0.931	18.9	1.028
PL HL 11.07.2022	15.7%	-20.0	-129.8	0.926	16.6	1.026
PL HL 01.08.2022	15.6%	-13.3	-139.3	0.913	16.5	1.025
PL HL 22.08.2022	10.8%	-25.3	-149.1	-	28.9	-
PL HL 05.09.2022	23.4%	-26.2	-146.3	0.903	9.4	1.017
PL HL 24.10.2022	25.3%	-26.8	-137.8	0.920	10.8	1.020
PL HL 05.12.2022	25.4%	-27.0	-139.8	0.919	16.1	1.025
PL VY 09.05.2022	23.6%	-27.2	-129.2	0.936	15.6	1.026
PL VY 30.05.2022	-	-	-	-	-	-
PL VY 22.06.2022	33.7%	-	-	-	-	-
PL VY 11.07.2022	31.6%	-27.6	-141.1	0.914	15.1	1.024
PL VY 01.08.2022	29.4%	-27.5	-147.1	0.904	24.8	1.033
PL VY 22.08.2022	23.9%	-27.4	-146.8	-	13.1	-
PL VY 05.09.2022	28.1%	-27.3	-146.0	0.903	28.1	1.036
PL VY 24.10.2022	-	-	-	-	-	-
PL VY 05.12.2022	-	-	-	-	-	-

A6: Stable isotopic signal ($\delta^{13}C$, $\delta^{2}H_n$, $\delta^{18}O_n$), the isotopic fractionation factors (α_{2H}, α_{18O}) and the weight percentage of carbon of the SHA component.

Sampling Site	% C	$\delta^{13}C$	$\delta^{2}H_n$	α_{2H}	$\delta^{18}O_n$	α_{18O}
PL 1 09.05.2022	27.9%	-26.2	-129.6	0.939	28.5	1.039
PL 1 30.05.2022	27.4%	-26.2	-131.4	0.935	24.5	1.035
PL 1 22.06.2022	29.7%	-26.2	-133.5	0.929	19.5	1.030
PL 1 11.07.2022	24.1%	-26.3	-130.1	0.924	18.4	1.027
PL 1 01.08.2022	25.0%	-26.4	-135.6	0.916	22.8	1.032
PL 1 22.08.2022	28.1%	-26.2	-135.0	-	21.7	-
PL 1 05.09.2022	-	-	-	-	-	-
PL 1 24.10.2022	16.7%	-26.3	-138.0	0.917	19.2	1.029
PL 1 05.12.2022	31.5%	-26.4	-131.6	0.932	25.6	1.036
PL dno 09.05.2022	6.4%	-26.5	-138.5	0.926	17.1	1.027
PL dno 30.05.2022	10.9%	-26.2	-141.6	0.923	31.8	1.042
PL dno 22.06.2022	10.1%	-26.4	-133.6	0.931	16.3	1.026
PL dno 11.07.2022	11.0%	-26.4	-142.0	0.922	26.3	1.037
PL dno 01.08.2022	9.2%	-26.5	-137.6	0.927	17.5	1.028
PL dno 22.08.2022	8.2%	-26.5	-135.5	-	23.8	-
PL dno 05.09.2022	7.2%	-26.6	-139.3	0.925	16.9	1.027
PL dno 24.10.2022	12.5%	-26.2	-126.6	0.940	21.5	1.032

PL dno 05.12.2022	11.9%	-26.3	-117.9	0.943	24.6	1.034
PL HL 09.05.2022	-	-	-132.0	0.933	39.5	1.050
PL HL 30.05.2022	7.5%	-26.8	-144.2	0.918	14.6	1.025
PL HL 22.06.2022	5.3%	-17.2	-154.5	0.902	16.4	1.025
PL HL 11.07.2022	7.0%	-10.0	-146.2	0.909	23.5	1.033
PL HL 01.08.2022	12.6%	-11.3	-158.0	0.894	22.8	1.031
PL HL 22.08.2022	10.5%	-25	-147.0	-	20.9	-
PL HL 05.09.2022	10.6%	-26.1	-142.6	0.907	10.0	1.018
PL HL 24.10.2022	6.2%	-26.4	-138.5	0.919	25.0	1.034
PL HL 05.12.2022	5.6%	-17.3	-75.6	0.988	16.6	1.026
PL VY 09.05.2022	-	-	-	-	-	-
PL VY 30.05.2022	-	-	-	-	-	-
PL VY 22.06.2022	-	-	-	-	-	-
PL VY 11.07.2022	10.2%	-25.2	-154.7	0.900	20.0	1.029
PL VY 01.08.2022	10.0%	-25.3	-157.4	0.893	20.3	1.028
PL VY 22.08.2022	12.1%	-24.9	-151.5	-	15.5	-
PL VY 05.09.2022	6.4%	-25.9	-140.9	0.909	8.6	1.016
PL VY 24.10.2022	-	-	-	-	-	-
PL VY 05.12.2022	-	-	-	-	-	-

A7: Hydrogen and oxygen isotopic signal (δ^2H, $\delta^{18}O$) from the water at the four sampling sites.

Sampling Site	δ^2H	$\delta^{18}O$
PL 1 09.05.2022	-73.34	-10.56
PL 1 30.05.2022	-71.00	-10.43
PL 1 22.06.2022	-67.40	-9.75
PL 1 11.07.2022	-58.49	-8.84
PL 1 01.08.2022	-56.74	-8.67
PL 1 22.08.2022	-	-
PL 1 05.09.2022	-57.91	-8.74
PL 1 24.10.2022	-59.65	-9.30
PL 1 05.12.2022	-67.88	-10.03
PL dno 09.05.2022	-69.57	-9.83
PL dno 30.05.2022	-69.96	-10.09
PL dno 22.06.2022	-69.31	-9.77
PL dno 11.07.2022	-69.44	-9.91
PL dno 01.08.2022	-69.77	-9.99
PL dno 22.08.2022	-	-
PL dno 05.09.2022	-70.00	-9.97
PL dno 24.10.2022	-70.71	-10.02
PL dno 05.12.2022	-64.96	-9.11
PL HL 09.05.2022	-69.93	-10.13
PL HL 30.05.2022	-67.75	-9.67
PL HL 22.06.2022	-63.05	-8.74
PL HL 11.07.2022	-60.55	-8.72
PL HL 01.08.2022	-57.67	-8.08
PL HL 22.08.2022	-54.75	-7.53

PL HL 05.09.2022	-	-
PL HL 24.10.2022	-62.72	-8.71
PL HL 05.12.2022	-64.40	-8.97
PL VY 09.05.2022	-69.73	-10.28
PL VY 30.05.2022	-68.70	-9.67
PL VY 22.06.2022	-63.40	-8.79
PL VY 11.07.2022	-60.40	-8.71
PL VY 01.08.2022	-56.96	-7.91
PL VY 22.08.2022	-54.60	-7.48
PL VY 05.09.2022	-	-
PL VY 24.10.2022	-62.12	-8.76
PL VY 05.12.2022	-61.45	-8.90

A8: Statistical results of the paired t-tests.

Test	α_{2H}	α_{18O}
Fractions:		
SPE-DOM & VHA	t(20)=12.026, p=1.309*10^{-10}	t(20)=0.223, p=0.8256
SPE-DOM & SHA	t(5)=-27.682, p=1.152*10^{-6}	t(5)=2.450, p=0.05797
VHA & SHA	t(5)=-4.4721, p=0.006566	t(5)=0.670, p=0.5323
Sampling Sites		
PL dno & PL 1	t(13)=-1.872, p=0.08383	t(13)=-0.871, p=0.3997
PL dno & PL HL	t(8)=2.584, p=0.03242	t(8)=2.357, p=0.04617
PL dno & PL VY	(9)=2.113, p=0.06375	t(9)=0.246, p=0.8114
PL 1 & PL HL	t(10)=10.262, p=1.253*10^{-6}	t(10)=1.564, p=0.1488
PL 1 & PL VY	t(11)=10.658. P=3.896*10^{-7}	t(11)=0.606, p=0.5565
PL VY & PL HL	t(8)=-2.8143, p=0.02269	t(8)=-0.863, p=0.4132

A9: Values of the three different EEM indices of the four sampling sites.

Sampling Date	Biological Index	Humification Index	Fluorescence Index
PL 1 11.07.2022	0.620	0.833	1.147
PL 1 01.08.2022	0.609	0.840	1.157
PL 1 22.08.2022	0.607	0.837	1.154
PL 1 05.09.2022	0.610	0.884	1.194
PL 1 24.10.2022	0.624	0.859	1.187
PL 1 05.12.2022	0.642	0.838	1.194
PL dno 11.07.2022	0.664	0.813	1.229
PL dno 01.08.2022	0.656	0.816	1.214
PL dno 22.08.2022	0.603	0.811	1.187
PL dno 05.09.2022	0.611	0.813	1.228
PL dno 24.10.2022	0.660	0.828	1.220
PL dno 05.12.2022	0.666	0.863	1.248
PL HL 11.07.2022	0.728	0.842	1.214
PL HL 01.08.2022	0.745	0.814	1.200
PL HL 22.08.2022	0.728	0.791	1.210
PL HL 05.09.2022	0.738	0.846	1.230
PL HL 24.10.2022	0.706	0.835	1.238
PL HL 05.12.2022	0.701	0.863	1.255

PL VY 11.07.2022	0.708	0.816	1.217
PL VY 01.08.2022	0.714	0.812	1.235
PL VY 22.08.2022	0.728	0.805	1.215
PL VY 05.09.2022	0.720	0.821	1.238
PL VY 24.10.2022	0.714	0.845	1.221
PL VY 05.12.2022	0.670	0.863	1.244

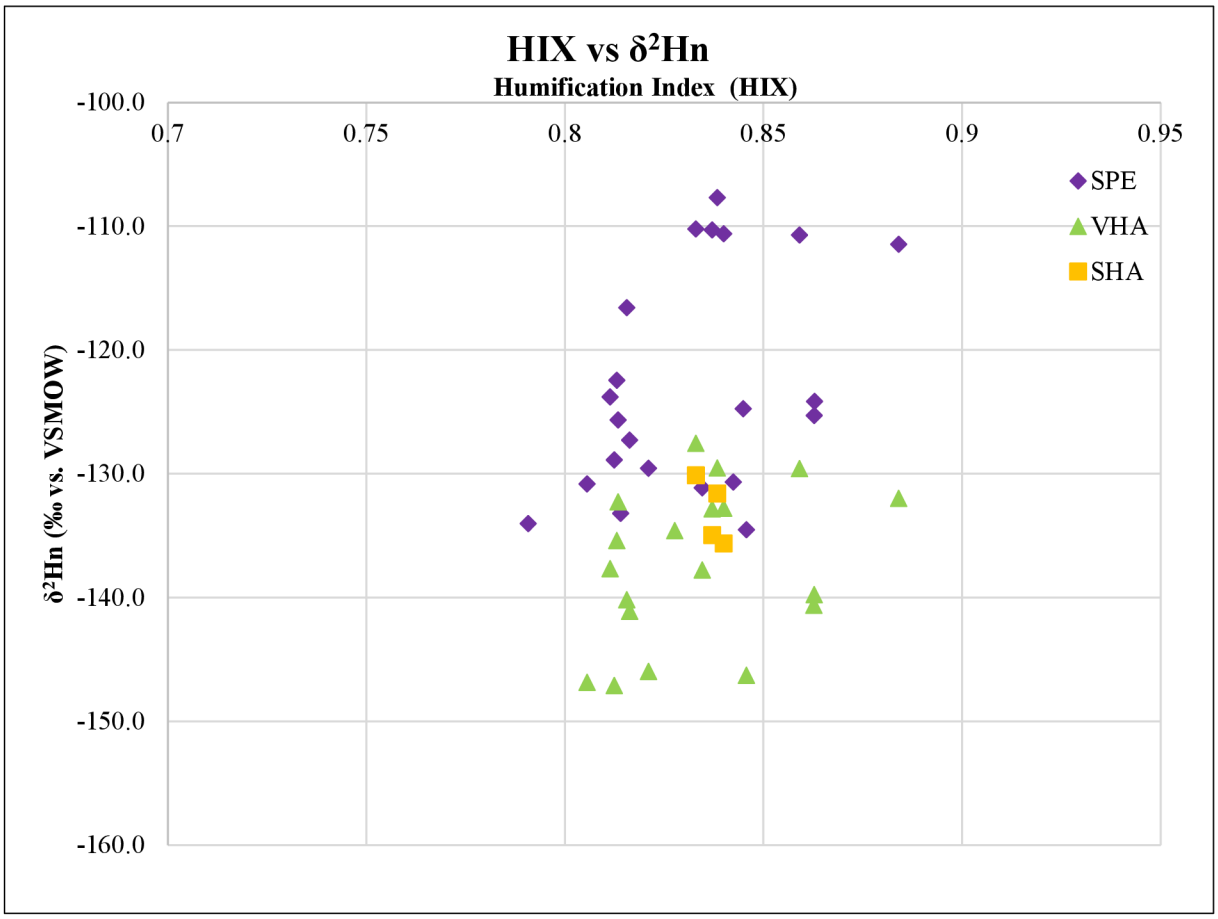

A10: δ^2H_n values from the three DOM fractions plotted against the humification index measured from the lake water.